Cell cycle entry triggers a switch between two modes of Cdc42 activation during yeast polarization

Kristen Witte, Devin Strickland, and Michael Glotzer

Dept. of Molecular Genetics and Cell Biology
University of Chicago
Chicago, IL 60637

Author for correspondence:
Michael Glotzer
mglotzer@uchicago.edu

Abstract

Cell polarization underlies many cellular and organismal functions. The GTPase Cdc42 orchestrates polarization in many contexts. In budding yeast, polarization is associated with a focus of Cdc42•GTP which is thought to self sustain by recruiting a complex containing Cla4, a Cdc42-binding effector, Bem1, a scaffold and Cdc24, a Cdc42 GEF. Using optogenetics, we probe yeast polarization and find that local recruitment of Cdc24 or Bem1 is sufficient to induce polarization by triggering self-sustaining Cdc42 activity. However, the response to these perturbations depends on the recruited molecule, the cell cycle stage, and existing polarization sites. Before cell cycle entry, recruitment of Cdc24, but not Bem1, induces a metastable pool of Cdc42 that is sustained by positive feedback. Upon Cdk1 activation, recruitment of either Cdc24 or Bem1 creates a stable site of polarization that induces budding and inhibits formation of competing sites. Local perturbations have therefore revealed unexpected features of polarity establishment.

Introduction

Cell polarization occurs in all kingdoms of life. In metazoa, it is critical for many cellular events including cell migration, embryogenesis, and cytokinesis. Polarization is dynamic, enabling cells to reorient to changing spatial and temporal cues. The central, conserved regulator of cell polarity in eukaryotes is the small Rho-family GTPase, Cdc42 (Johnson and Pringle 1990; Etienne-Manneville 2004; Macara 2004). Establishment of an axis of polarity frequently involves the accumulation of active Cdc42 at a unique position on the cell cortex. An initial cue induces Cdc42-GTP accumulation at a unique site, where it then concentrates via an amplification system. This amplification system maintains the polarity site (Thompson 2013). While this general scheme of polarity establishment is fairly well established, the dynamic molecular interactions required for establishing, maintaining, and enforcing a single axis of polarity are not well understood.

One of the best studied cell polarization systems is bud site selection in *Saccharomyces cerevisiae*. Wild type yeast cells use landmark-directed cues to define the polarization axis (Figure 1A). However, cells lacking these spatial cues or the GTPase that transduces these cues, Rsr1, efficiently establish polarity in a process known as symmetry breaking. The current model of symmetry breaking suggests that stochastic accumulation of Cdc42-GTP induces a positive feedback loop mediated by a polarity complex containing the Cdc42 GEF, Cdc24, the scaffold protein, Bem1, and Cla4, which binds directly to activated Cdc42 (Howell et al. 2012) (Figure 1B). This tripartite complex is required for polarity establishment and its molecular features provide the requisite domains to result in positive feedback (Chenevert et al. 1992; Holly and Blumer 1999; Bose et al. 2001; Butty et al. 2002). Computational models and in vivo analyses of symmetry breaking have uncovered behaviors consistent with positive feedback, including traveling waves and oscillatory accumulation of polarity proteins (Ozbudak, Becskei, and Van Oudenaarden 2005; Howell et al. 2012). However, important assumptions of the

models have not been directly tested. For instance, whenever Cdc42 is active it should induce accumulation of the polarity complex; however, the validity of this critical assumption has yet to be established. Similarly, although the events preceding bud emergence have been dissected in considerable detail, the events that precede those have attracted relatively little attention. For example, in symmetry breaking polarization, do events in early G1 influence the site of symmetry breaking? To what extent are the functions of the polarity proteins influenced by the state of the cell cycle? These omissions are largely due to the absence of tools that permit controlled perturbation of Cdc42 activation.

In recent years, a number of genetically-encoded tools have been developed that allow control of diverse proteins using light (Tischer and Weiner 2014). We have developed a set of small, highly engineered optogenetic protein tags, called TULIPs, that permit light-mediated control of protein-protein interactions (Strickland et al. 2012). In this system, the optically-responsive protein (LOVpep) is tethered to the plasma membrane whereas its cognate binding partner (ePDZ) freely diffuses in the cytoplasm. Illumination induces a conformational change in LOVpep that allows it to bind ePDZ, causing the rapid (< 10 sec) relocation of ePDZ to the membrane. LOVpep spontaneously relaxes to the dark state with a half-time of 80 sec (Strickland et al. 2012). By fusing a protein of interest to ePDZ, we can potently and dynamically control its spatiotemporal localization using light. In previous proof of principle experiments, we demonstrated that local recruitment of Cdc24 directs formation of a mating projection in α-factor treated cells (Strickland et al. 2012).

Using optogenetic tools, we have probed the mechanism for yeast cell polarization. Our results provide direct evidence that positive feedback contributes to polarity establishment once Cdk1 is activated at START. However, while the current model predicts that the polarity components invariably function together in a potent positive feedback loop, we find that they do not do so prior to Cdk1 activation and that Cdc42 activation does not invariably induce the canonical

positive feedback loop. Rather, we demonstrate the existence of a second positive feedback loop involving Cdc24 that precedes the canonical loop and appears to function independently of Bem1. Finally, we show that multiple nascent sites of polarization compete, and that this competition is particularly potent upon activation of the Bem1-dependent positive feedback loop. We conclude that two alternative modes of positive feedback function in concert to promote polarity initiation and establishment, with their respective behaviors regulated under strict cell cycle control.

Results

Cdc24 recruitment can activate Cdc42 in both unpolarized and polarized cells

In order to probe the mechanism of cell polarization, we developed optogenetic tools to recruit yeast polarity proteins to defined sites on the cell cortex. Specifically, we co-expressed a membrane-tethered variant of LOVpep (Mid2-GFP-LOVpep) with either Bem1-ePDZ or Cdc24-ePDZ in diploid *rsr1Δ* cells. In all conditions, the TULIPs-tagged proteins were expressed under the control of a β-estradiol inducible promoter (Louvion, Havaux-Copf, and Picard 1993), and the ePDZ-tagged polarity component was expressed in addition to its endogenous counterpart. We perturbed cells by illuminating at a single site with a diffraction-limited laser. The response to this perturbation was examined by following the recruitment of a Cdc42 biosensor derived from the Cdc42 effector protein Gic2 (Tong et al. 2007) and Nomarski optics to observe bud emergence.

We first examined the ability of Cdc24 and Bem1 to bias the site of polarization in unpolarized cells as a function of illumination frequency. We measured the angle, θ, between the site of illumination and the position of the nascent bud. These values were linearly scaled such that budding at the center of the laser target was assigned a score of 1 and budding opposite the target was assigned a score of -1; these scores were averaged for a population of cells (Polarization Efficiency = average(1-2θ/π)) (Figure 1D). Recruitment of Cdc24 or Bem1

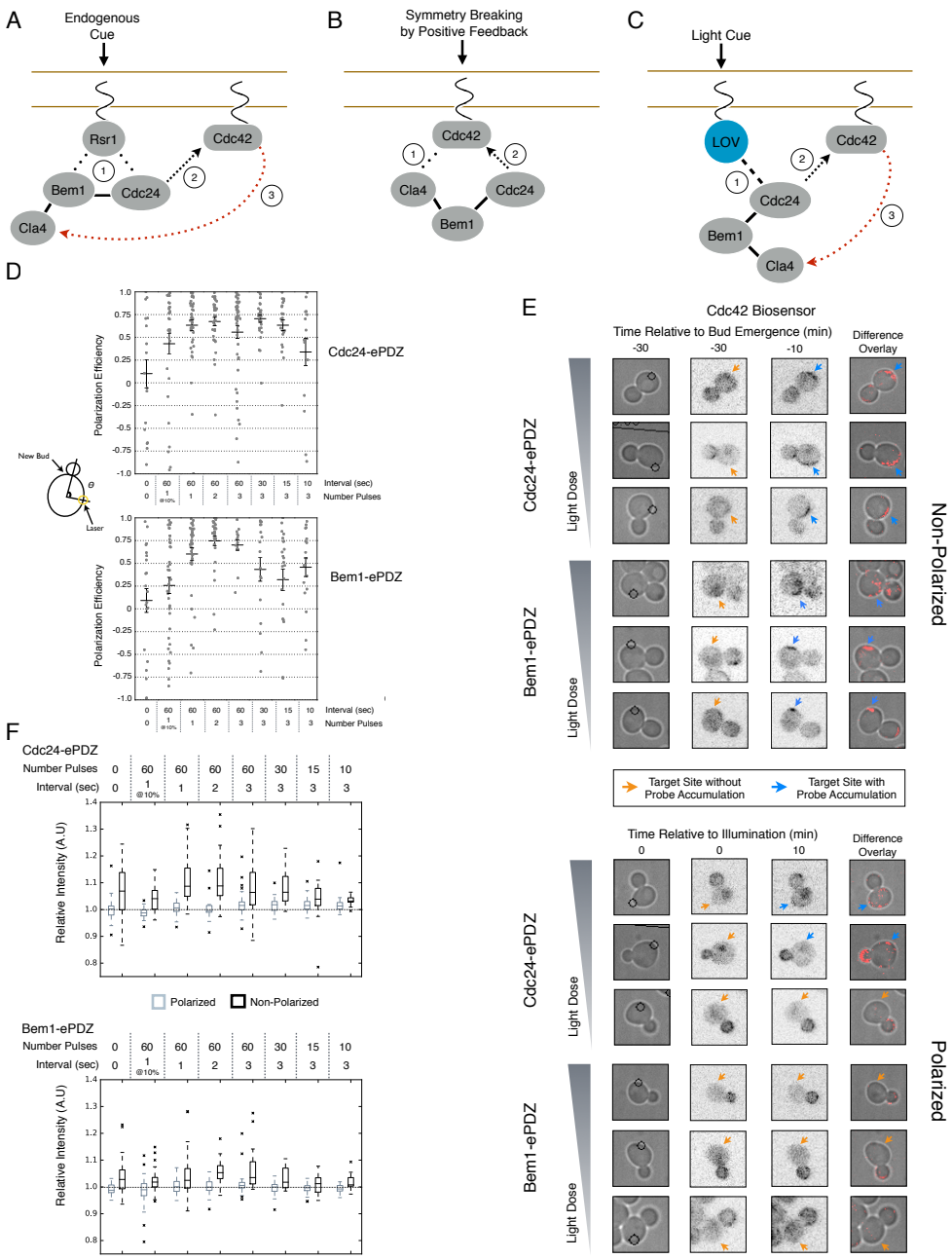

Figure 1: Cdc24 can activate Cdc42 in both polarized and unpolarized cells.
A) The endogenous cue is mediated by a system involving Rsr1 to yield patterned budding. Rsr1 directly interacts with Bem1 and Cdc24 to recruit and activate Cdc42 at an adjacent bud position. Rsr1 recruits Bem1 and/or Cdc24 **(1)** to activate Cdc42 **(2)** adjacent to the previous bud neck. Cdc42 undergoes positive feedback **(3)** by interacting with Cla4 to promote its own accumulation.
B) In the absence of Rsr1, cells undergo a symmetry breaking event mediated by positive feedback. The symmetry breaking event may involve a stochastic accumulation of Cdc42-GTP at a unique location that then recruits the Cla4-Bem1-Cdc24 complex **(1)**. Cdc24 activates additional molecules of Cdc42 **(2)** to promote positive feedback **(3)**.
C) Light-induced symmetry breaking by recruiting the GEF Cdc24 to activate Cdc42 at a prescribed position and induce positive feedback. Localized photo-activation of LOVpep recruits Cdc24-ePDZb **(1)** to activate Cdc42 **(2)**. Activated Cdc42 interacts with Cla4 to induce positive feedback.
D) Polarization efficiency of a population of cells where each point represents an individual cell. The angle ɵ is defined by the angle between the site of bud emergence and the laser position. Data are averages of all cells across multiple experiments (n experiments > 2, N total cells > 25 for each group). Average and +/- SEM is indicated. Statistical analysis in Figure 1 - Supplemental Figure 1.
E) Representative phase and inverted fluorescent images depicting the activation of Cdc42 in response to either Cdc24 or Bem1 recruitment in polarized or non-polarized cells. Difference overlay images place the subtraction of the two fluorescent images overlaid onto the phase contrast image. An increase in fluorescent signal is depicted by red psuedo-coloring on the overlay. Cells were treated to increasing doses of light. Shown from bottom to top, representative images for each group:1 pulse/60 sec, 3 pulses/30 sec, and 3 pulses/15 sec.
F) Box-and-Whisker plots depicting the relative change in mean fluorescence intensity of the Cdc42 biosensor at targeted regions. The relative intensity of polarized cells is the mean of the intensity at 10 minutes post initial illumination compared to the intensity prior to illumination. The relative intensity for non-polarized cells compares activation of the biosensor 10 minutes before bud emergence relative to the intensity prior to illumination. Data is combined across multiple experiments (n experiments > 2, N total cells > 25 for each group). Statistical analysis in Figure 1 - Supplemental Figure 3.

recruitment was able to bias the bud site at very low light doses; Bem1 was slightly more efficient than Cdc24 (Figure 1D). Additionally, recruitment of either component induced robust accumulation of active Cdc42 at the site of illumination, without altering the timing of polarization (~95 minutes between bud emergence events, regardless of photo-activation state or molecule recruited; data not shown). As the frequency of light increased, the ability of Cdc24 to bias the bud site remained roughly constant until the highest light dose, while the polarization efficiency of Bem1 dropped by ~50% once illumination increased to greater than 3 pulses per minute (Figure 1F, Figure 1 - Supplemental Figure 1). The reason for this drop is unclear. While symmetry breaking is predicted to be random relative to the previous bud site, the position of the new bud was not completely random. Additionally, targets were not randomly positioned, as the area around the previous bud site was underrepresented. These biases would cause a slight underestimation of polarization efficiency (Figure 1 - Supplemental Figure 2). Optogenetically recruited Cdc24 and Bem1 were also able to induce polarization of heterozygous *RSR1/rsr1Δ* diploids (Figure 1 - Supplemental Figure 3).

We next assessed how the response varied as a function of both cell cycle position and the frequency with which cells were illuminated. At all doses of light, cells that were at the start of the cell cycle (~10 minutes before bud emergence) activated Cdc42 in response to both Cdc24 and Bem1 recruitment. Some non-illuminated cells also exhibited Cdc42 activation at the target site, as the bud site occasionally coincided with the target position (Figure 1D, F). To determine whether cells were constitutively responsive to optogenetic recruitment of Cdc24 or Bem1, we illuminated polarized cells with small to medium-sized buds. At infrequent light pulses, polarized cells did not activate Cdc42 in response to Cdc24 or Bem1 recruitment (1-3 pulses, Figure 1E, F, Figure 1-Supplemental Figure 3). When cells were illuminated at a greater frequency (>2x per minute), those that expressed Cdc24-ePDZ activated detectable Cdc42 at all stages of the cell cycle. Conversely, Bem1 recruitment did not result in Cdc42 activation in polarized cells, even at

higher illumination frequencies (Figure 1E, F, Figure 1-Supplemental Figure 4). In summary, Cdc42 activation in unpolarized cells is readily attained in response to either Cdc24 or Bem1 recruitment; however, only high levels of Cdc24 recruitment can generate Cdc42-GTP in polarized cells, indicating that limitations to Cdc42 activation exist in polarized cells.

From these data, we conclude that local recruitment of either Cdc24 or Bem1 is able to efficiently bias the bud site. Because our primary interests lie in the endogenous regulation of Cdc42 activation, we chose to dissect polarity establishment using a light dose (3 pulses per minute) that efficiently biases the bud site, rather than the higher doses that might overcome the mechanisms that limit Cdc42 activation to one site in the cell.

Bem1 recruitment induces positive feedback

To understand the role of Bem1 in regulating polarization, we induced Bem1 recruitment in cells expressing either the Cdc42 biosensor, Cdc24-tdTomato expressed on a low-copy plasmid from its endogenous promoter, or cells in which one copy of Bem1 was tagged with tdTomato. Optogenetic recruitment of Bem1 was sufficient to promote activation of Cdc42, accumulation of Cdc24 (Figure 2A, B), and was able to efficiently position the bud site (Figure 2D). Critically, we found that recruitment of Bem1 was able to induce the accumulation of endogenous Bem1 at the prescribed site, directly showing that polarization in yeast proceeds via positive feedback (Figure 2A, B). These results raise the possibility that the observed activation of Cdc42 represents a combination of the direct activation of Cdc42 by the Cdc24 directly interacting with optogenetically-recruited Bem1 and amplification by endogenous mechanisms. Although Bem1 recruitment efficiently induced cell polarization, it did not induce precocious Cdc42 activation, or recruitment of Cdc24 or Bem1 as compared to control cells (Figure 2B, Figure 2 - Supplemental Figure 1). Thus, the activity of the Cdc24-Bem1-Cla4 feedback loop appears sensitive to cell cycle regulation.

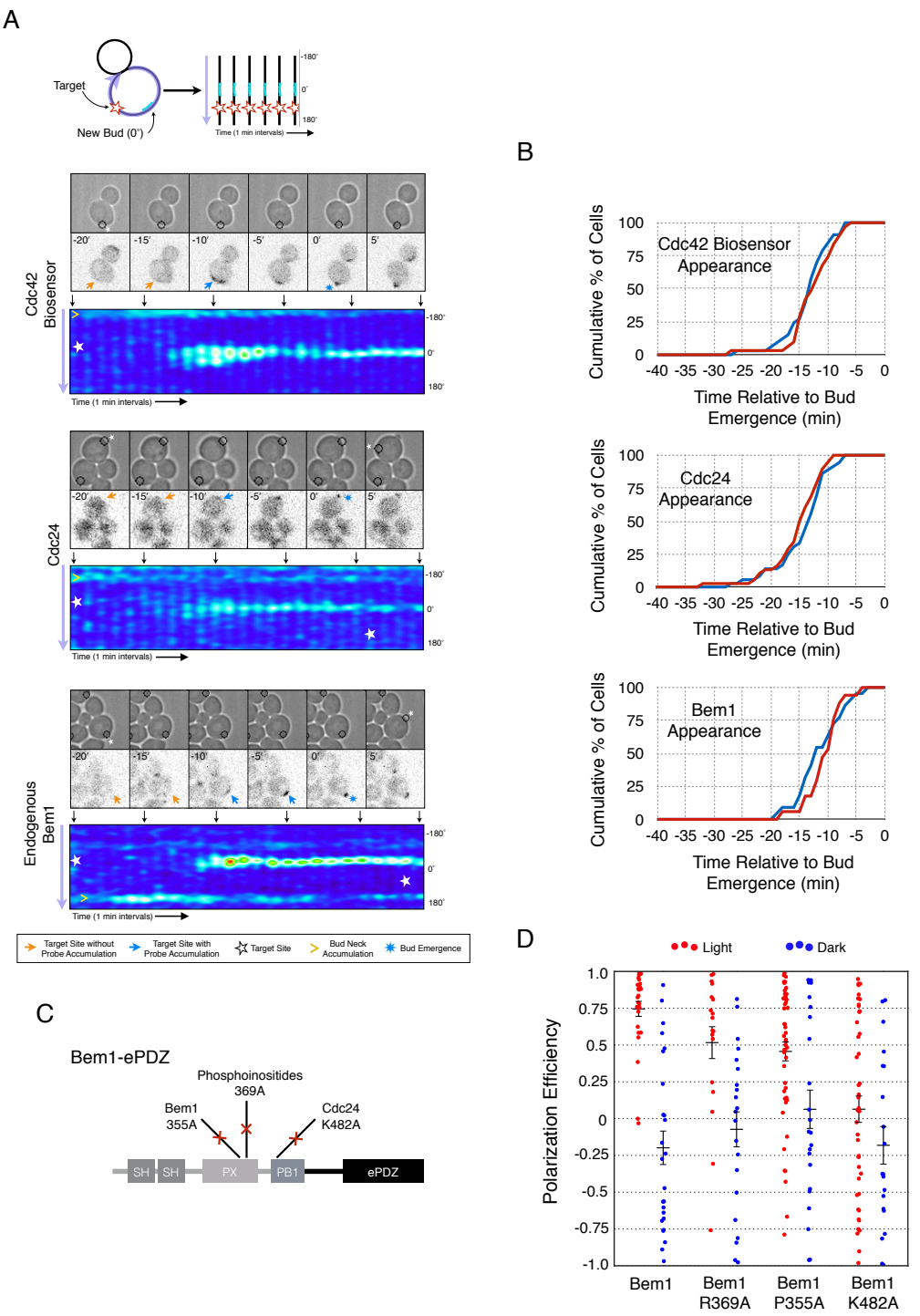

Figure 2: Local accumulation of Bem1 is sufficient to bias the bud site.

A) Representative phase and fluorescence images and kymographs showing the position of the laser target and accumulation of the Cdc42 biosensor, Cdc24, and endogenous Bem1 (respectively). Kymographs are generated by iteratively linearizing the membrane at each time point (schematic). Bud emergence occurs at Y = 0° and at time = 0 minutes. Arrows between the kymograph and fluorescent images correlate to the time shown in the panels.

B) Accumulation kinetics for each component in response to Bem1 recruitment. Red line is photo-activated cells, blue line is mock-illuminated cells. Bud emergence is time = 0. Data combined across multiple experiments (n experiments > 2, N total cells > 30 for each condition).

C) Domain schematic of Bem1-ePDZ, with mutation sites and interactions.

D) Polarization efficiency of a population of cells as in **1F.** Red dots are single photo-activated cells. Blue dots are single mock-illuminated cells. Data is combined across multiple experiments (n experiments > 2, N total cells > 20 for each group). Error bars S.E.M. polarization efficiency of Bem1, Bem1 R369A, and Bem1 P355A in the light was statistically significant relative to Bem1 K482A light and dark, and their respective dark-state controls. Bem1 K482A was not statistically significant relative to its dark state control. $p < 0.05$, Mann-Whitney *U* test.

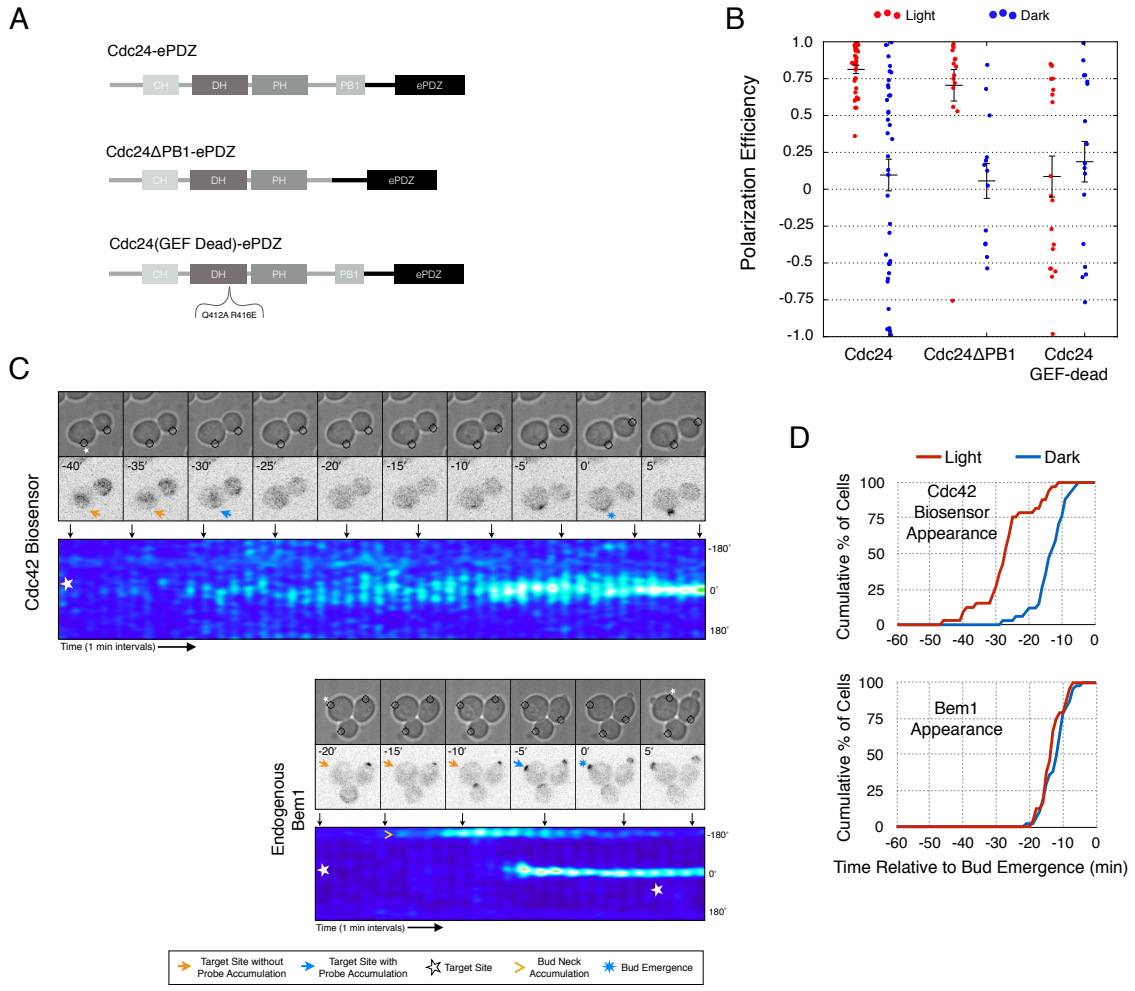

Figure 3: Light-mediated recruitment of Cdc24 is sufficient to induce symmetry breaking
A) Domain schematic of Cdc24-ePDZ, with mutation sites and interactions.
B) Polarization efficiency of photo-illuminated (red) or mock-illuminated (blue) cells. Data are averaged across multiple experiments (n experiments > 2, N total cells > 20, for each group). Average and +/- S.E.M. indicated. polarization efficiency of Cdc24 and Cdc24ΔPB1 were statistically significant relative to Cdc24-GEF-dead light/dark, and statistically significant compared to their respective dark state controls. The difference between Cdc24 and Cdc24ΔPB1 were not statistically significant. The response to Cdc24-GEF dead was not statistically significant relative to its dark state control. $p < 0.05$, Mann-Whitney *U* test.
C) Panels of representative phase and fluorescence images and kymographs showing the position of the laser target and accumulation of a Cdc42 biosensor or endogenous Bem1 in response to Cdc24 recruitment.
D) Accumulation kinetics for the Cdc42 biosensor or endogenous Bem1 in response to Cdc24 recruitment. Data are combined across multiple experiments (n experiments > 2, N total cells > 30 for each condition).

If polarization induction by Bem1 proceeds via a positive feedback loop, Bem1 likely functions by directly interacting with the GEF Cdc24 (Kozubowski et al. 2008). To test this prediction, we introduced a mutation in the Bem1 PB1 domain that has previously been shown to abolish the Bem1-Cdc24 interaction (K482A) (Figure 2C) (Irazoqui, Gladfelter, and Lew 2003) and tested its ability to induce cell polarization. Mutational inactivation of the Bem1 PB1 domain ablated its

polarization efficiency (Figure 2D). In addition to its Cdc24-interacting domain, Bem1 contains a region that mediates homo-oligomerization as well as a region demonstrated to interact with phosphoinositides (PI) (Figure 2C). We introduced mutations known to abolish these activities (Irazoqui, Gladfelter, and Lew 2003) and assayed each for their ability to bias the bud site. While both functional domains were required for full activity, mutation of the oligomerization domain (P355A) was more detrimental than mutation of the PI-binding region (R369A) (Figure 2D). These results suggest that polarity induction by Bem1 requires direct interaction with Cdc24. Furthermore, they indicate that the most active form of Bem1 is likely a dimer or oligomer, at least in *rsr1Δ* cells (Irazoqui, Gladfelter, and Lew 2003). Although the PI-binding region is required for Bem1 function (Irazoqui, Gladfelter, and Lew 2003), light-mediated recruitment or indirect recruitment of endogenous Bem1 might compensate for this defect in this assay. We conclude that yeast polarization polarization involves a positive feedback loop mediated by the Bem1-GEF complex. Furthermore, these data indicate that bud site selection requires activation of Cdc42.

Cdc24 recruitment induces precocious activation of Cdc42

To gain a mechanistic understanding of light-induced polarity establishment in response to recruitment of Cdc24 GEF, we determined which molecular features are required for induction of cell polarization (Figure 3A, B). In addition to GEF activity, Cdc24 also contains a PB1 domain that enables it to bind to a corresponding PB1 domain on Bem1 (Butty et al. 2002). Recently, it has been suggested that localization of Cdc24 is required for polarization via its ability to activate Cdc42 (Woods et al. 2015). As expected, we find that mutation of conserved surface residues in the GEF-GTPase interface (Rossman et al. 2002) rendered Cdc24 inactive for polarization activity (Figure 3A, B) and Cdc42 activation (data not shown). Deletion of the Bem1-binding domain of Cdc24 marginally reduced the polarization efficiency of the GEF (Figure 3A, B). These results indicate that local recruitment of Cdc24 polarizes yeast cell growth through its

ability to activate Cdc42, and that the interaction of the recruited Cdc24 with other cellular proteins - including endogenous wild-type Cdc24 - is not sufficient to induce polarization.

To observe the dynamics of Cdc42 activation in response to optogenetic Cdc24 recruitment, we used the biosensor of active Cdc42 to visualize GTPase activation (Figure 3C, Video 1). In control cells, 50% of cells displayed Cdc42 activation 12 minutes prior to bud emergence (Figure 3D, Figure 3 - Supplemental Figure 1). In experiments in which Cdc24 was continuously recruited, we observed precocious Cdc42 activation; 50% of cells exhibited polarized accumulation of active Cdc42 27 minutes prior to bud emergence (Figure 3C, D). Precocious Cdc42 activation was less robust than that observed in the ~12 minutes prior to bud emergence. Thus, Cdc24 recruitment can induce Cdc42 activation at an earlier stage in the cell cycle than Bem1.

We next asked whether endogenous Bem1 precociously accumulated in a similar manner as activated Cdc42. Strikingly, Bem1 did not accumulate until ~13 minutes prior to bud emergence (Figure 3C, D). Indeed, despite accumulation of active Cdc42 as a consequence of Cdc24 recruitment, Bem1 accumulates at the same time relative to bud emergence in illuminated and mock-illuminated cells (-13 minutes and -12 minutes, respectively) (Figure 3D, Figure 3 - Supplemental Figure 1). Notably, the initial accumulation of Bem1 coincides with the time in which more robust Cdc42 activation is observed. These results suggest that, unlike previous models for the activity of the polarity proteins, Cdc42 activation does not invariably lead to recruitment of the intact polarity complex.

Cdc24, Bem1, and Cdc42 do not constitutively colocalize

The differential accumulation of Bem1 and Cdc42 in response to optogenetic recruitment of Cdc24 indicates that Cdc24 has the potential to activate Cdc42 independently of Bem1, and that activated Cdc42 does not inevitably induce recruitment of the polarity complex. If this is the case, then Cdc24, Bem1, and Cdc42-GTP may not constitutively colocalize in non-perturbed

cells. To test this hypothesis, we performed a detailed colocalization analysis of the three pairwise combinations of active Cdc42, Bem1, and Cdc24. In all strains expressing fluorescent Bem1, one copy of endogenous Bem1 was tagged. The Cdc42 biosensor was used to assess the pool of active Cdc42. To visualize Cdc24, we transformed cells with a low-copy plasmid encoding an extra copy of Cdc24-GFP under its own promoter. Though it localizes to the expected sites and it can be readily detected, Cdc24-GFP was dimmer than Bem1-tdTomato, Bem1-GFP, and the Cdc42 biosensor.

Using imaging conditions optimized for detection of faint signals (see Materials and Methods), we acquired maximum intensity Z-projections of asynchronous cells. Using bud size and polarization as a guide, we sub-divided the cells into unbudded G1 cells, small-budded cells, and large-budded cells and characterized the localization pattern of each pair of probes in each cell cycle state. Unbudded cells were subdivided into two groups: early and late. Early cells were characterized by small distinct puncta of all three probes. Late cells featured a wide, cortically associated band in which all three probes localized. The categorization of these patterns as early and late is substantiated by previous studies (Ozbudak, Becskei, and Van Oudenaarden 2005) and time-lapse imaging (see below, Figure 4C).

As expected, all three probes colocalize at the tips of small and nascent buds. However, at other stages of the cell cycle Bem1, Cdc24, and active Cdc42 do not colocalize (Figure 4A). In large-budded cells, activated Cdc42 and Bem1 localize throughout the growing bud, while the GEF is limited to the growing bud tip. Additionally, puncta of the Cdc42 biosensor are detected in the mother cell. In early G1 cells, Bem1 and Cdc24 each localize in cortically associated puncta, but surprisingly, these puncta do not overlap. Furthermore, both Bem1 puncta and Cdc24 puncta displayed limited overlap with the Cdc42 biosensor, with only 35% and ~50% of puncta colocalizing, respectively (Figure 4B, Figure 4 - Supplemental Figure 1). Non-overlapping puncta were also in seen single plane snapshots of each pairwise combination (Figure 4 -

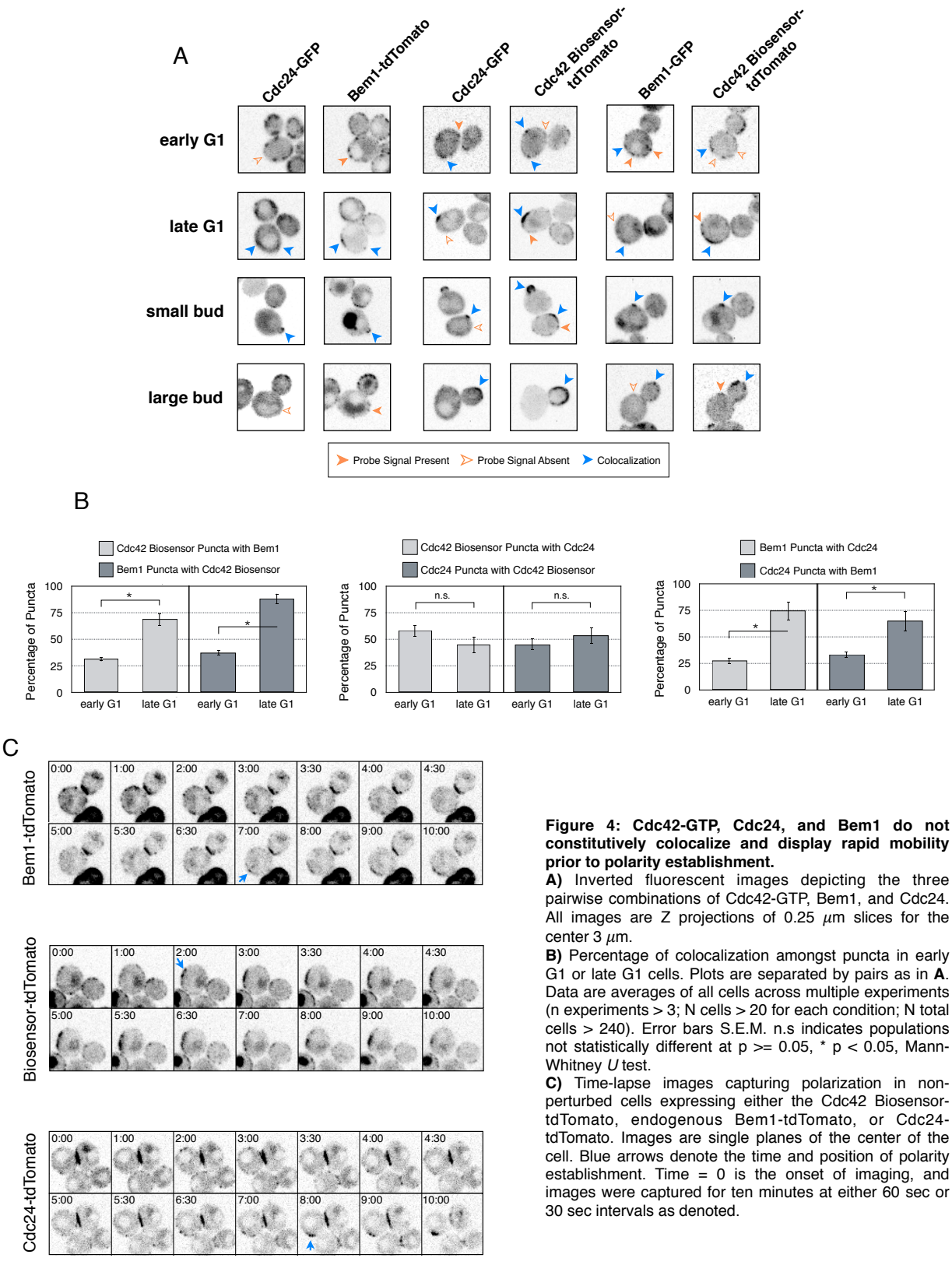

Figure 4: Cdc42-GTP, Cdc24, and Bem1 do not constitutively colocalize and display rapid mobility prior to polarity establishment.

A) Inverted fluorescent images depicting the three pairwise combinations of Cdc42-GTP, Bem1, and Cdc24. All images are Z projections of 0.25 μm slices for the center 3 μm.

B) Percentage of colocalization amongst puncta in early G1 or late G1 cells. Plots are separated by pairs as in **A**. Data are averages of all cells across multiple experiments (n experiments > 3; N cells > 20 for each condition; N total cells > 240). Error bars S.E.M. n.s indicates populations not statistically different at p >= 0.05, * p < 0.05, Mann-Whitney *U* test.

C) Time-lapse images capturing polarization in non-perturbed cells expressing either the Cdc42 Biosensor-tdTomato, endogenous Bem1-tdTomato, or Cdc24-tdTomato. Images are single planes of the center of the cell. Blue arrows denote the time and position of polarity establishment. Time = 0 is the onset of imaging, and images were captured for ten minutes at either 60 sec or 30 sec intervals as denoted.

Supplemental Figure 2). Notably, the localization pattern shifted in late G1 cells as all three components localize to the wide band, and the amount of reciprocal overlap between Bem1-Cdc24 and Bem1-Cdc42 biosensor increased to greater than 70% (Figure 4B, Figure 4 - Supplemental Figure 1). This more extensive overlap amongst Cdc24, the Cd42 biosensor, and Bem1 in late G1 cells suggest that prior to the onset of polarization, Cdc24 has the potential to function independently of Bem1. Of note, the punctate patterns of Bem1 and Cdc42 seen in early G1 cells are below the limit of detection in the assays involving optogenetic recruitment. Exposure times in those experiments were far lower in order to limit photobleaching during long-term (>90 minutes) imaging.

To better understand the variation in protein localization at different cell cycle stages, we complemented the static imaging with time-lapse imaging. As proteins tagged with GFP tended to be dimmer than those tagged with tdTomato, we imaged cells expressing the tdTomato-tagged variants of the Cdc42 biosensor, Bem1, or Cdc24. Asynchronous populations of cells were imaged for a total of 10 minutes; images were acquired more frequently during the central four minutes. Each component was highly dynamic in the minutes leading up to the formation of a prominent wide band of accumulation, confirming that the punctate stage precedes polarization. While some puncta existed in the same spot for up to 3 minutes, appearance and disappearance of puncta were common (Figure 4C).

These results indicate that the majority of Cdc24 and Bem1 molecules are not in a constitutive complex during early G1, which is consistent with the finding that recruitment of Cdc24, but not Bem1, induces Cdc42 activation at this stage of the cell cycle. Cell cycle regulated assembly of the polarity complex could readily explain both results.

Cdk1 activation is required for Bem1 accumulation

To gain insight into cell cycle regulation of the polarity complex, we performed Cdc24 recruitment studies in strains co-expressing a marker of cell cycle entry, Whi5-tdTomato, and

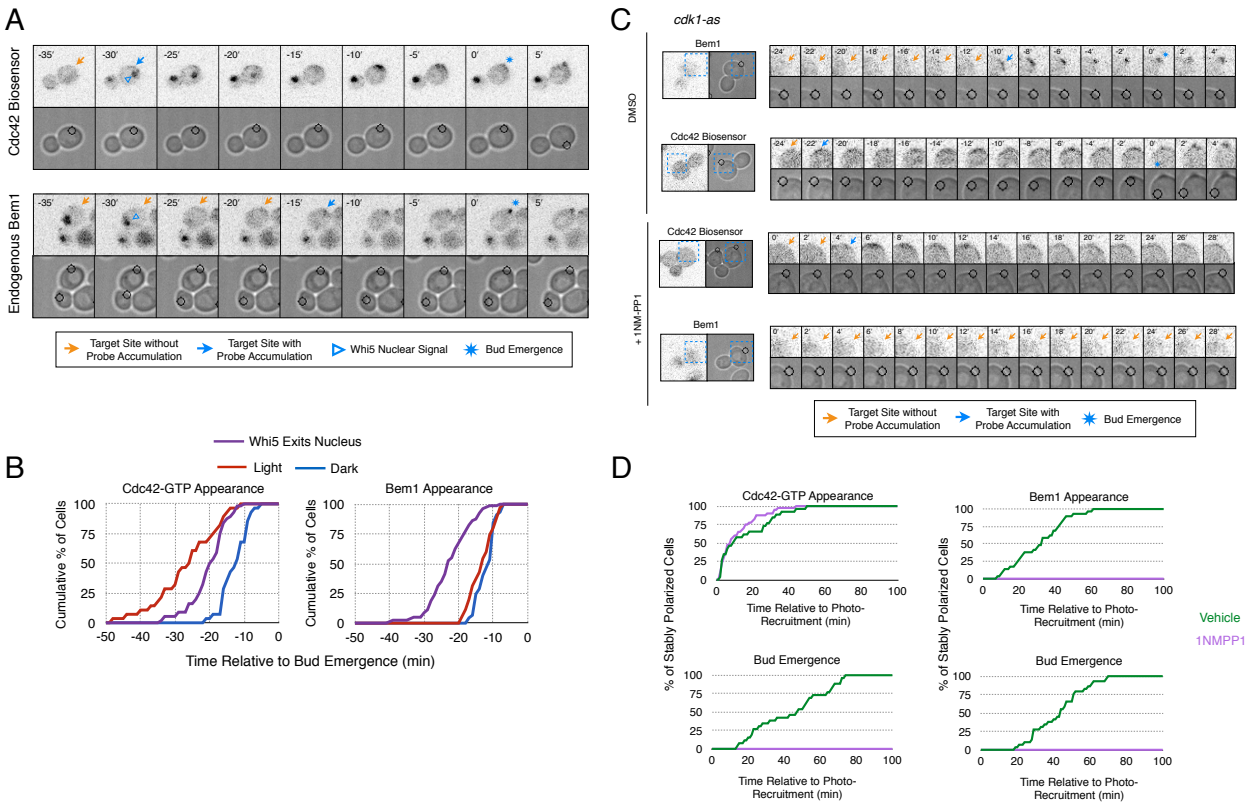

Figure 5: Cdk1 activation is required for Bem1 accumulation, but dispensable for Cdc42 activation.
A) Representative panel of time-course images from Cdc24 recruitment in cells co-expressing Whi5-tdTomato with either the Cdc42 biosensor or Bem1-tdTomato.
B) Whi5 nuclear exit kinetics and accumulation kinetics for either Cdc42 activation or Bem1 at Cdc24 recruitment sites. Purple line represents Whi5 exit, with data combined for both light- and dark-state conditions as they are not significantly different (Figure 5 - Supplemental Figure 1). Bud emergence occurs at time = 0. Data are combined across multiple experiments (n experiments > 2; N total cells > 30 for each condition).
C) Representative panels and sub-images of cells depicting the response to Cdc24 recruitment +/- Cdk1 activity.
D) Accumulation plots indicating the response of Cdc42 biosensor or Bem1 in response to Cdc24 recruitment +/- Cdk1 activity. Purple lines represent cells treated with 75 μM 1NM-PP1. Green lines represent Vehicle-treated cells. Data are combined across multiple experiments (n experiments = 2; N total cells > 40 for each condition).

either the Cdc42 biosensor or Bem1-tdTomato. Nuclear import of Whi5 is a marker of Cdk1 inactivation. Whi5 is concentrated in the nucleus during the interval between mitotic exit until Cdk1 activation at Start (Costanzo et al. 2004; Skotheim et al. 2008) (~25 minutes prior to bud emergence, Figure 5 - Supplemental Figure 1). Recruitment of Cdc24 can induce local Cdc42 activation in cells containing nuclear Whi5. Polarized accumulation of active Cdc42 precedes Whi5 nuclear export (Figure 5A, B). In contrast, cortical recruitment of Bem1-tdTomato did not occur until ~12 minutes after Whi5 nuclear exit, corresponding to ~13 min prior to budding

(Figure 5A, B, Figure 5 - Supplemental Figure 2). These results are consistent with a model in which Cdk1 activation is required for the Bem1-GEF complex to engage active Cdc42.

To directly test whether Cdk1 activation is required for Bem1 recruitment in response to active Cdc42, we utilized an allele of Cdk1 that can be inhibited by an ATP-analog (cdk1-as1 and 1NM-PP1, respectively) (Bishop et al. 2000; McCusker et al. 2007). Asynchronous cells were pre-treated with 1NM-PP1 for 20 minutes and we subsequently monitored the ability of Cdc24 to induce Cdc42 activation or Bem1 accumulation in recruitment assays. We limited our analysis to mother cells with large-budded daughter cells, indicative of mother cells in early G1. Consistent with previous reports (McCusker et al. 2007), cells lacking Cdk1 activity could not undergo bud emergence nor could buds grow significantly (Figure 5C, D). Nevertheless, Cdc24 recruitment induced accumulation of Cdc42 in 67% of Cdk1-inhibited cells (data not shown). Indeed, Cdc42 was activated with the same kinetics irrespective of the presence or absence of the inhibitor (Figure 5D). Strikingly, when Cdk1 activity was suppressed, Bem1 failed to accumulate within the time frame of the experiment (greater than 1.5 hours after addition of 1NM-PP1) (Figure 5C, D, Figure 5 - Supplemental Figure 3). Furthermore, when Bem1 was recruited, cells were unable to activate Cdc42 within the time frame of the experiment (data not shown). Cells expressing wild-type *cdk1* were unaffected by the addition of 1NM-PP1 (Figure 5 - Supplemental Figure 4). These results demonstrate that Cdk1 activation is required for both Bem1 accumulation and bud emergence even in cells with locally activated Cdc42.

Cdc24 recruitment induces a Bem1-independent positive feedback loop

A prominent model for positive feedback posits that the Bem1-GEF complex is constitutive (Bose et al. 2001). However, our data indicates that, prior to Cdk1 activation, optogenetically-recruited Cdc24 and Bem1 function differently. The ability of Cdc24 to activate Cdc42 in the apparent absence of Bem1 lacks precedent; therefore we studied the characteristics of these optogenetically-initiated sites. Specifically, we sought to determine the stability of these sites

and whether these nascent sites of polarization interact. To answer these questions, we exploited the ability of the optogenetic system to dynamically reposition the site of protein recruitment.

During the time window between the transition from isotropic growth and the time at which Cdc24 recruitment triggers Bem1 accumulation (i.e. ~13 minutes prior to bud emergence), Cdc24 recruitment can induce Cdc42 activation. To test whether these sites are self sustaining, the targets were removed after Cdc42 activation was detected in early G1. Optogenetic recruitment of ePDZ-tagged proteins is largely reversed within 3 minutes after discontinuing illumination (Strickland et al. 2012), ensuring that any remaining signal is not due to Cdc24-ePDZ remaining at the target site due to the optogenetic tag. The region retained a faint but consistent signal of active Cdc42 for up to 30 minutes and ultimately resulted in budding from the specified site (Figure 6A, B). Conversely, Bem1 recruitment was only sufficient to bias the bud site if it was recruited within 15 minutes of bud emergence (Figure 6A, B). This observation shows that Cdc42 activity can be maintained at a unique site in the apparent absence of Bem1-mediated positive feedback. Thus optogenetic recruitment of Cdc24 can induce a self-sustaining pool of Cdc42 activation.

To determine how optogenetically induced Cdc42 activation could be maintained in the absence of the optogenetic cue, we tested whether recruited Cdc24 induces a change in the localization of cytosolic Cdc24. To that end, we recruited Cdc24 and visualized Cdc24-tdTomato. Indeed, optogenetically-recruited Cdc24-ePDZ altered the distribution of Cdc24-tdTomato in unpolarized cells (Figure 6C). Specifically, in 50% of cells in which Cdc24-ePDZ was recruited, Cdc24-tdTomato appeared on the cortex ~25 minutes before bud emergence, whereas in mock-illuminated cells, Cdc24-tdTomato appeared on the cortex ~15 minutes before bud emergence (Figure 6D, Figure 6 - Supplemental Figure 1). The kinetics of accumulation for Cdc24-tdTomato parallels that of activated Cdc42 in response to Cdc24 recruitment (Figure 3). From these data

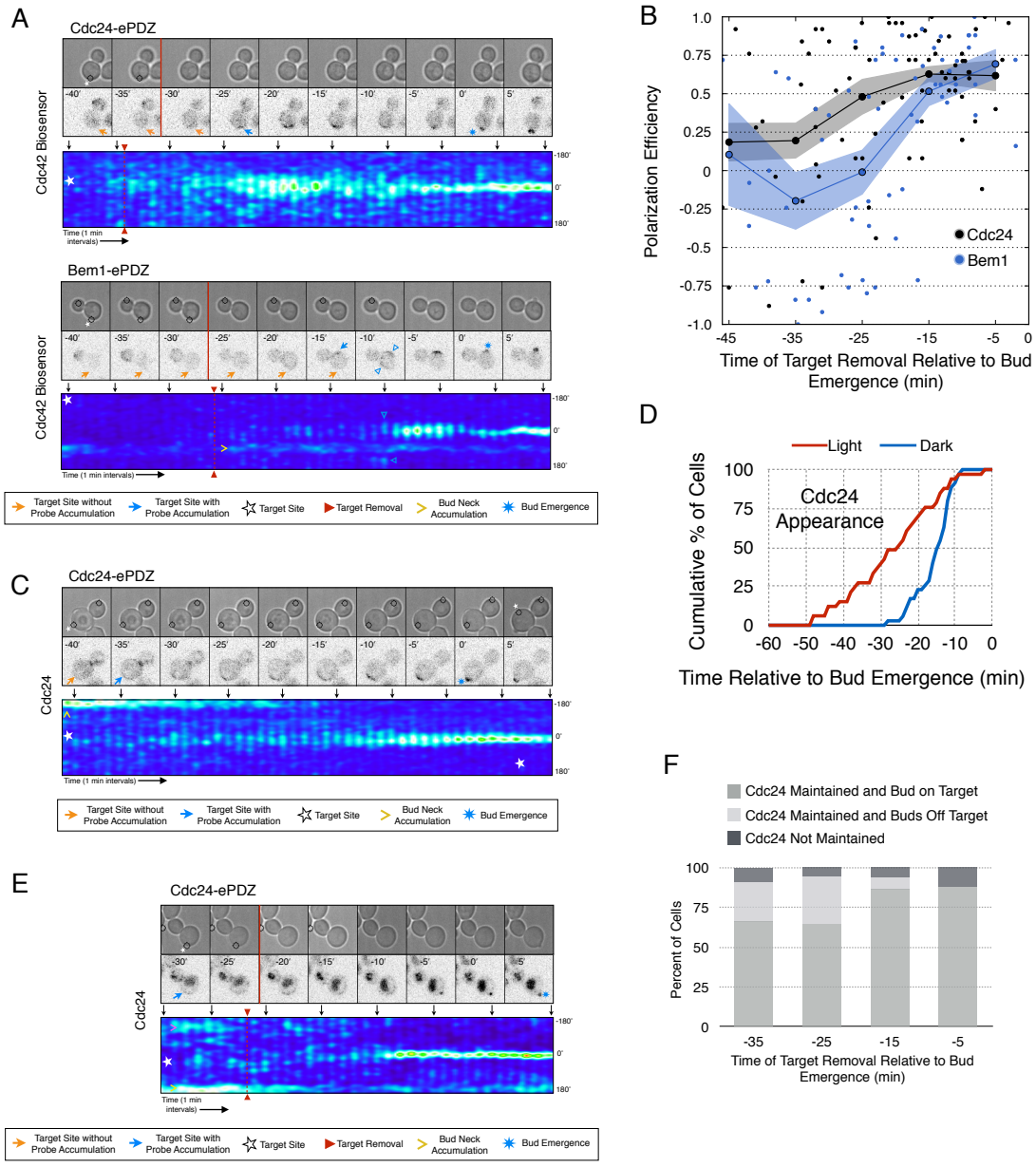

Figure 6: Cdc24 recruitment induces precocious Cdc42 activation and Cdc24-tdTomato accumulation that is self-sustaining.
A) Phase and fluorescence images and kymographs of representative cells depicting the response to the transient recruitment of Cdc24-ePDZ or Bem1-ePDZ. Initial target site denoted by white stars.
B) Polarization efficiency following transient recruitment of Cdc24 and Bem1. Time indicates when the target was removed relative to bud emergence (bud emergence occurs at time = 0). Black dots represent polarization of individual cells in response to transient Cdc24 recruitment. Blue dots represent polarization of individual cells in response to transient Bem1 recruitment. Lines represent averages (+/- SEM) of data binned in 10 min intervals, with the middle time point represented on the plot. Results are pooled across multiple experiments (n experiments > 3; N cells > 10 for each time interval; N total cells > 75). Polarization Efficiencies of Cdc24 at -5, -15, and -25 min and Bem1 at -5 and -15 min were statistically significant relative to all earlier time points. Cdc24 and Bem1 Polarization Efficiencies were not statistically different at -45, -35, -15, and -5 min. $p < 0.05$, Mann-Whitney *U* test.
C) Representative phase and fluorescence images and kymographs showing the position of the laser target and accumulation of Cdc24-tdTomato in response to Cdc24-ePDZ recruitment.
D) Accumulation kinetics for Cdc24-tdTomato. Data are combined across multiple experiments (n experiments > 2, N total cells > 30 for each condition).
E) Panels of representative phase and fluorescence images indicating the response of Cdc24-tdTomato to transient Cdc24-ePDZ recruitment. Orange arrows denote sites of illumination without Cdc24-tdTomato accumulation. Purple arrowhead indicates erroneous signal from vacuole.
F) Stacked bar chart indicating the percentage of cells that maintain Cdc24-tdTomato accumulation in response to Cdc24 recruitment and whether they polarize to the prescribed site. Data is binned by 10 minute time intervals, with the middle time point represented on the plot. Data combined across multiple experiments (n experiments > 3, N total cells > 25 for each condition).

we conclude that recruitment of Cdc24 can induce both Cdc42 activation and Cdc24 recruitment prior to Cdk1 activation, both of which appear to occur independently of Bem1. Collectively, these results reveal the existence of a second pathway for positive feedback. The observed activation of Cdc42 likely represents a combination of direct Cdc42 activation by optogenetically recruited Cdc24 and its amplification by endogenous mechanisms.

Given that Cdc24-tdTomato accumulates at nascent sites, we hypothesized that it would remain at sites after the optogenetic cue was halted by removal of the target. Intriguingly, we observed Cdc24 was maintained at the site for ~6 minutes following cessation of optogenetic perturbation (Figure 6E). After this 6 minute time window, the Cdc24 signal became more punctate and these puncta dynamically associated with the previously targeted region. Greater than 65% of cells budded from the targeted region when target removal occurred ~30 minutes prior to bud emergence (Figure 6F). In cells that budded from sites outside the targeted region, Cdc24 was maintained at the targeted region until ~15 minutes before bud emergence when an intense focus of Cdc24 would appear at a new site that would ultimately form the bud (Figure 6, Supplemental Figure 2). These data indicate that optogenetically-initiated sites of Cdc42 activation are stable and are maintained, at least in part, by the accumulation of Cdc24, without accumulation of detectable Bem1.

Nascent sites interact during early G1

To examine whether two sites of active Cdc42 in early G1 cells compete with one another, the target was repositioned within the same cell. Repositioning of the target caused Cdc42 accumulation at a new site and concomitant dissipation from the old site, with Cdc42 activity simultaneously detected at both sites for ~5 minutes (Figure 7A, Video 2). However, the site of Cdc42 accumulation could not be continuously repositioned. A qualitative change in behavior occurs prior to bud emergence. When targets are repositioned within ~13 min of bud emergence, accumulation of Cdc42 at the initial site remains and Cdc42 accumulates weakly at

the new site. The cell eventually buds from the site where Cdc42 was active at the ~13 minute transition point and Cdc42 signal from the alternate site dissipates upon bud emergence (Figure 7B). Our previous results demonstrate that Bem1 begins to accumulate at the targeted site ~13 minutes before bud emergence. To confirm that the basis for the qualitative switch relied on the ability of Cdc24 recruitment to induce Bem1 accumulation, we performed the same experiment in cells expressing Bem1-tdTomato. As previously shown, Bem1 only detectably accumulated at the target position defined at the ~13 minute transition point and it did not accumulate at new sites if the target was repositioned prior to bud emergence (Figure 7C, D). These results indicate that activation of the Bem1-dependent positive-feedback loop stabilizes sites of Cdc42 activation. Furthermore, these data suggest that prior to Cdk1 activation, nascent sites of polarization influence Cdc42 activation at other sites.

Given that Bem1 accumulation at Cdc24-prescribed sites requires Cdk1 activation, we hypothesized that the dynamic properties of Cdc24-generated sites would persist in the absence of Cdk1 activation. To test this prediction, we repeated the experiment in cells expressing *cdk1-as* treated with 1NM-PP1 (Figure 7E). Again, limiting our analysis to mother cells with large-budded daughter cells, we found that Cdc42 activation could be dynamically repositioned for >70 minutes and that Bem1 was not detectably recruited within this time (Figure 7E, F). These results confirm that Cdk1 activation is required for Bem1-mediated positive feedback activity, which functions to establish the axis of polarity.

Combined, these results support three conclusions: (i) the ability of active Cdc42 to induce Bem1 accumulation is cell cycle regulated, (ii) once active, the canonical positive feedback loop is highly stable and it prevents Cdc42 activation at competing sites, and (iii) maintenance of active Cdc42 and cytosolic Cdc24 before cell cycle entry appears independent of Bem1; therefore, the GTPase and the GEF participate in a positive feedback mechanism that functions earlier than the canonical Bem1-dependent positive feedback loop. This alternative positive

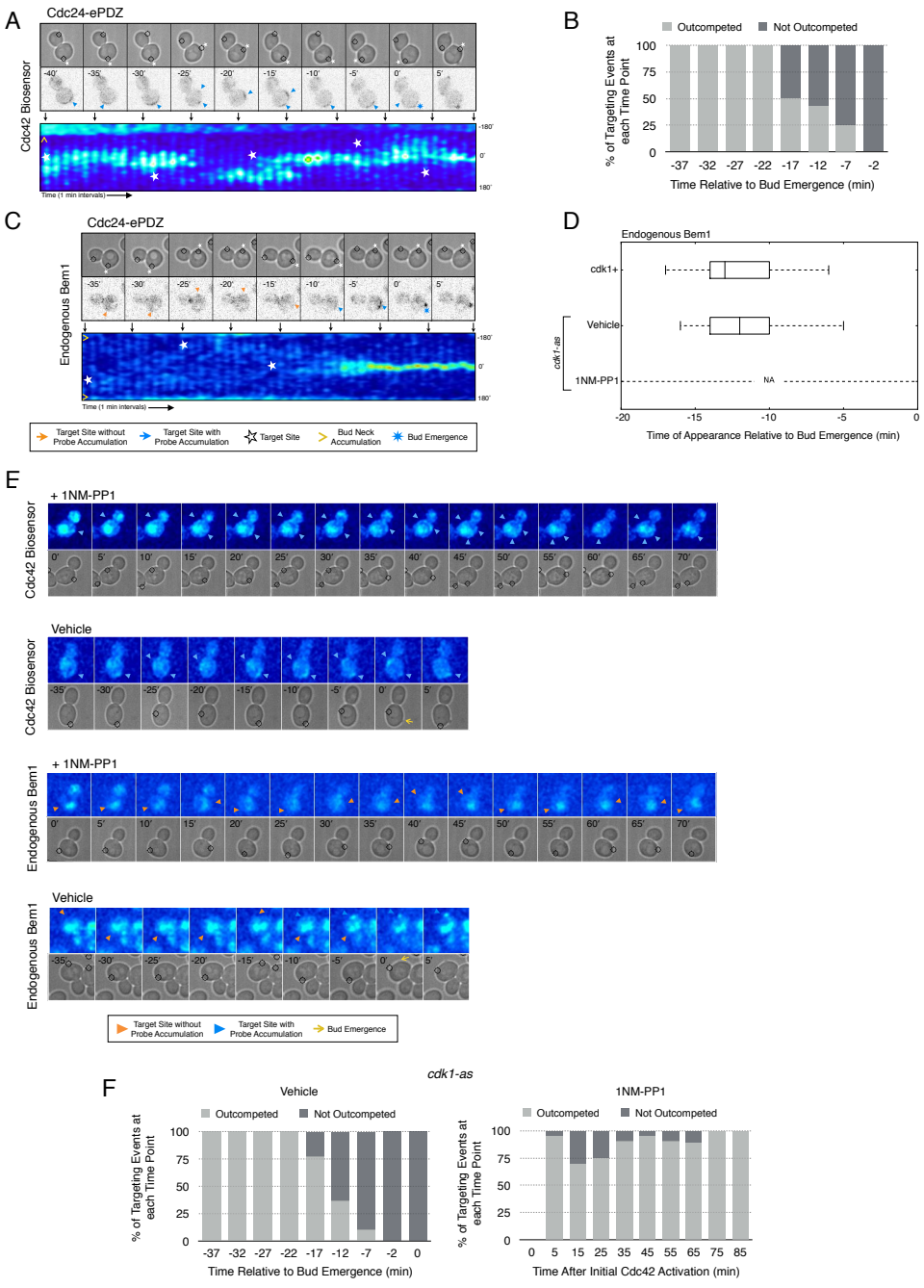

Figure 7: Local Cdc24 recruitment induces precocious activation of Cdc42 that is dynamically maintained in the apparent absence of Bem1.

A) Panels of representative cells depicting the response to dynamically re-positioned Cdc24 recruitment. Upper panels consist of phase contrast and fluorescent images and the lower panel is a kymograph. The laser was moved every 10 +/- 2 minutes throughout the cell cycle, as denoted by the white stars.

B) Percentage of targeting events "Outcompeted" or "Not Outcompeted" relative to bud emergence (Time = 0). Time indicates when the target was moved to a new position relative to bud emergence. Data is binned by 5 minute time intervals, with the middle time point represented on the plot. The event was scored as "outcompeted" if Cdc42 activity dissipated from the original position and accumulated at the new position. Conversely, the event was scored as "not outcompeted" if Cdc42 activity remained at the initial position upon target repositioning. Data are combined across multiple experiments (n total experiments > 2; n targeting events per time interval > 10; N total targeting events > 100; N total cells > 20).

C) Panels and a kymograph of a representative cell depicting the accumulation of Bem1 in response to dynamically re-positioned Cdc24 recruitment.

D) Box-and-whisker plot denoting Bem1 accumulation in CDK1, *cdk1-as* + DMSO, and *cdk1-as* + 1NM-PP1 cells.

E) Time-course images of *cdk1-as* cells challenged with Cdc24 dynamic reorientation. Panels consist of phase contrast and either Cdc42-GTP or Bem1 accumulation psuedo-colored as a heat map. Cells were treated with either DMSO or 1NM-PP1 as denoted.

F) Quantification of dynamic reorientation in vehicle-treated or 1NM-PP1-treated *cdk1-as* cells. Described in **B**.

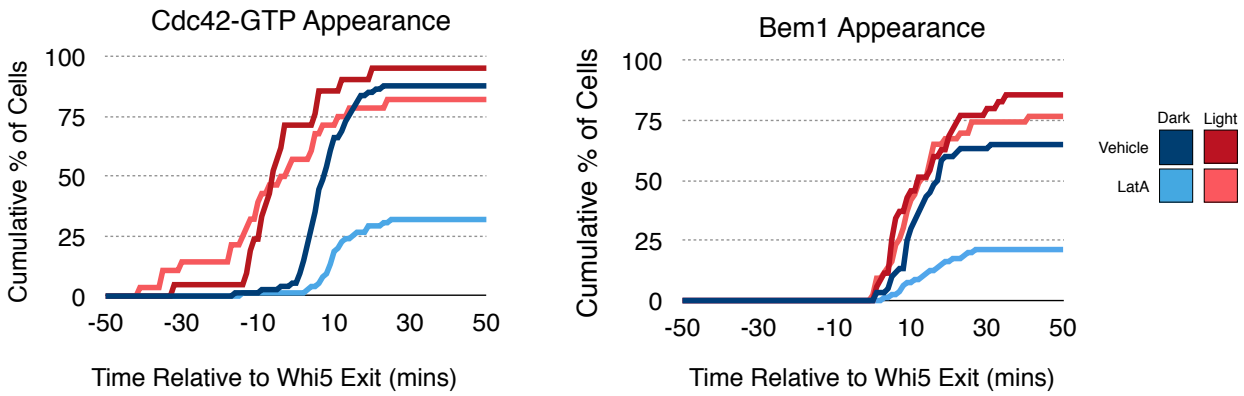

Figure 8: Localized recruitment of Cdc24 can overcome the polarity defect caused by actin depolymerization. Accumulation kinetics for Cdc42-GTP or Bem1 in response to Cdc24 recruitment in the presence or absence of polymerized actin. All cells scored as "polarized" also undergo bud emergence within the course of the experiment (>100 minutes). Red lines represent cells exposed to light-induced Cdc24 recruitment. Blue lines represent mock-illuminated cells. Dark lines represent Vehicle-treated cells, while lighter-colored lines represent Latrunculin A-treated cells (see schematic).. Whi5 nuclear exit was used as a cell cycle marker and accumulation of Cdc42-GTP or Bem1 was scored relative to Whi5 exit. Data was binned by 5 minute intervals and combined across multiple experiments (n experiments = 2; N total cells > 40).

feedback mechanism can be readily competed by a new site of Cdc24 recruitment; however, its existence suggests it could play a physiological role in establishing Cdc42 activity before Start in diploid cells.

Actin plays a limited role in Cdc42 activation

As F-actin has been proposed to play a role in polarity establishment (Wedlich-Soldner et al. 2003; Freisinger et al. 2013; Jose et al. 2013), we examined whether actin depolymerization affects the response induced by local recruitment of Cdc24. Cells expressing light-recruitable Cdc24, Whi5-tdTomato and either the Cdc42 biosensor or Bem1-tdTomato were partially synchronized in G1 using a nocodazole block and release protocol and treated with Latrunculin A (LatA) to depolymerize F-actin. As previously shown, actin depolymerization partially inhibited cell polarization (Jose et al. 2013). While 88% of cells polarize Cdc42-GTP in the presence of f-actin, only 32% of cells polarize when actin is depolymerized (Figure 8). Actin depolymerization has a similar effect on the efficiency of Bem1-tdTomato polarization. Drug treatment also slows cell cycle entry as judged by the efficiency of Whi5 exit from the nucleus (Figure 8—figure supplement 1), indicating that actin depolymerization affects several cellular processes.

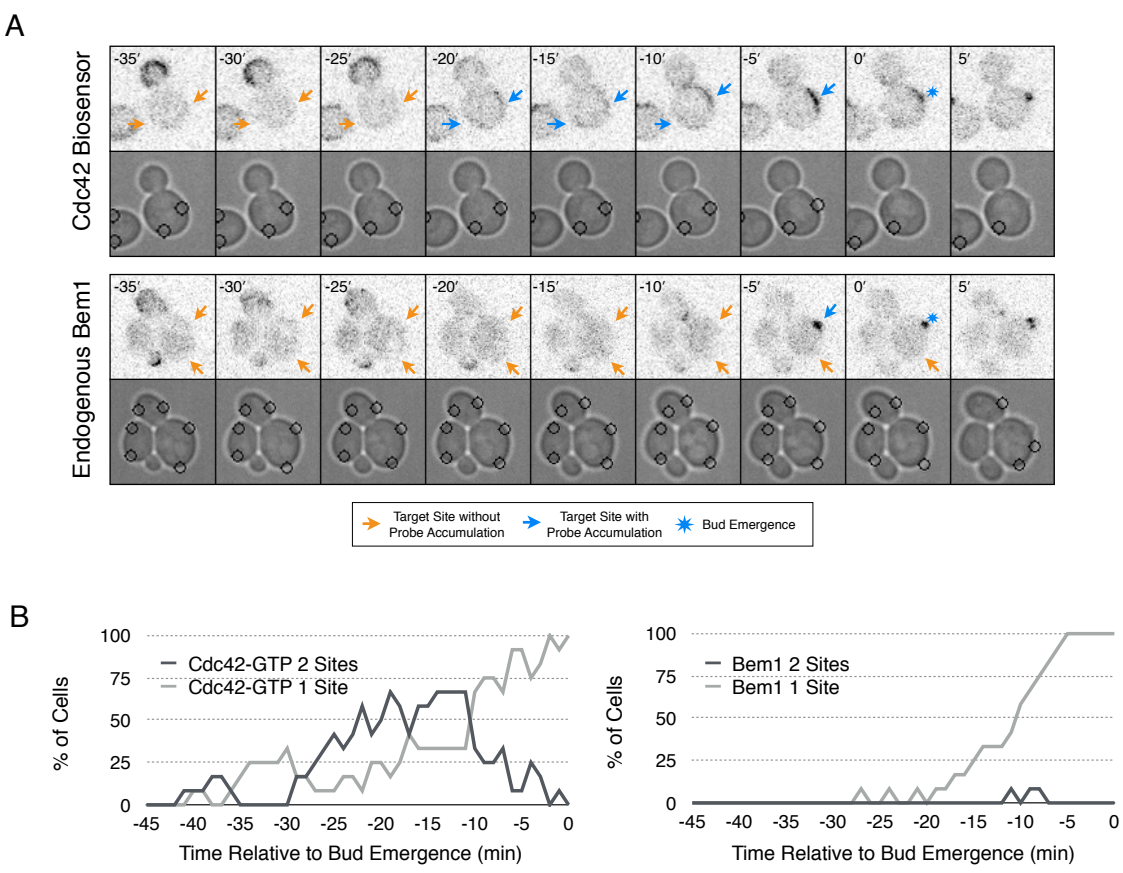

Figure 9: Nascent sites undergo competition to establish a single axis of polarity.
A) Representative fluorescence and phase images in response to recruitment of Cdc24 to two sites simultaneously. Top panel depicts Cdc42-GTP response. Bottom panel depicts Bem1 response.
B) Percentage of cells with signal at one or both sites at any given time relative to bud emergence. Dark gray lines depict percentage of cells with activation at two sites simultaneously. Light gray lines represent percentage of cells with accumulation at only a single site. Bud emergence occurs at time = 0. Data are combined across multiple experiments (n experiments > 2; N total cells > 30 for each condition).

Filamentous actin has been suggested to facilitate delivery of Cdc42 to the cortex where it could be activated by Cdc24 (Wedlich-Soldner et al. 2003). If true, Cdc24 recruitment would not be predicted to correct the polarization defect. However, light-directed recruitment of Cdc24 dramatically increased the fraction of cells that locally accumulate Cdc42-GTP in the absence of actin. Similarly, Bem1 polarization was rescued by Cdc24 recruitment in cells treated with LatA (Figure 8). These results suggest that actin depolymerization does not appear to affect the availability of Cdc42, but rather it impacts the localization of the Bem1-Cdc24 complex, perhaps non-specifically.

Two sites compete to establish an axis of polarity

In the previous experiments, only one Cdc24-targeted site was active at the moment when Cdk1 was activated resulting in activation of Bem1-mediated positive feedback loop. Cdc24 recruitment to multiple sites at this critical time might result in recruitment of Bem1 at multiple sites, leading to the formation of multiple buds. Alternatively, sites may compete with each other as they form resulting in only one site becoming fully established. Therefore, to investigate whether nascent sites also interact, we recruited Cdc24 to two sites simultaneously in unpolarized cells. Both sites generated activated Cdc42 (Figure 9A, Video 3) and retained active Cdc42 until ~11 minutes before bud emergence. Subsequently, Cdc42 activity was limited to only one site (Figure 9B) and bud emergence occurred at that site. In a parallel experiment with recruited Cdc24, we monitored accumulation of Bem1 and observed that it accumulates at only one of the two sites, which invariably predicted the site of bud emergence (Figure 9A, B, Video 4). Furthermore, despite recruitment of Bem1 to two sites simultaneously, in the overwhelming majority of cases (31/33 cells), Cdc42 activation and Bem1 accumulation occurred at one site, which ultimately defined the nascent bud (data not shown). These results indicate that multiple sites cannot coexist after activation of the Bem1-mediated positive feedback loop even under conditions in which they are simultaneously specified.

Discussion

In this work, we have studied the mechanism for Cdc42 activation throughout G1. Traditional genetic and cell biological analyses have identified the key components and revealed many behaviors associated with cell polarization, which have led to a set of models that invoke positive feedback (Wedlich-Soldner et al. 2003; Irazoqui, Gladfelter, and Lew 2003; Goryachev and Pokhilko 2008; Howell et al. 2012; Howell and Lew 2012). However, the field has lacked the tools that can directly interrogate the spatio-temporal dynamics of signaling molecules and

critically test the models. Here, we used optogenetics to probe the endogenous regulatory mechanisms that control Cdc42 activity. We used low light doses to recruit limited amounts of Cdc24 to reproducibly induce cell polarization; these conditions only resulted in Cdc42 activation at specific cell cycle stages. Rather than examining the direct consequences of experimentally induced GTPase activation (Wagner and Glotzer 2016), we sought to generate small perturbations and define the conditions in which those perturbations were amplified by the endogenous pathways. Using this approach, we have demonstrated the existence of a previously postulated positive feedback loop which promotes bud emergence. In addition, we have demonstrated that potent mechanisms ensure that only a single site can undergo positive feedback at a given time. We have also found that the activity of this pathway is temporally confined by cell cycle regulation. Finally, we have demonstrated the existence of a second, previously uncharacterized, positive feedback mechanism that can maintain a focus of Cdc42 activity prior to Cdk1 activation and which may play a role in symmetry breaking polarization.

Positive feedback in yeast polarity

The current model of symmetry breaking polarization posits that a stochastic accumulation of Cdc42-GTP activates a positive feedback loop mediated by the Cla4-Bem1-Cdc24 polarity complex, thereby generating a local focus of activated Cdc42 (Howell and Lew 2012). A prediction of that model is that a seed of Cdc42-GTP would be sufficient to define the nascent bud site. We find that local, light-induced recruitment of either the GEF Cdc24 or the scaffold Bem1 is sufficient to bias the presumptive bud site (Figure 1). Furthermore, the ability of these proteins to induce polarization requires the molecular features necessary to generate active Cdc42; specifically, GEF activity for Cdc24 and Cdc24-binding ability for Bem1 (Figure 3 and Figure 2, respectively). These findings are consistent with the existing model for symmetry breaking, in which a positive feedback loop modulated by the polarity complex reinforces local activation of Cdc42 to promote bud emergence. We present direct evidence for positive

feedback by optogenetically recruiting Bem1 and showing that endogenous Bem1 accumulates in response to that perturbation. Likewise, Cdc24 recruitment generates positive feedback by recruiting additional molecules of Cdc24 (Figure 6). Unexpectedly, we find that the GEF Cdc24 functions in two distinct positive feedback pathways; the Bem1-dependent loop that is active upon Cdk1 activation, and an earlier, positive feedback mechanism that appears to be Bem1 independent. The molecular mechanism of positive feedback during early G1 remains to be identified. It may involve Cdc24 oligomerization (Mionnet, Bogliolo, and Arkowitz 2008), however it is likely more complex as GEF-dead Cdc24 fails to induce Cdc42 activation or polarity establishment, suggesting Cdc42 also plays a role in this process.

Other models for symmetry breaking polarization invoke actin-dependent delivery of Cdc42 to the cortex (Wedlich-Soldner et al. 2003; Freisinger et al. 2013; Jose et al. 2013). While depolymerization of actin does induce a polarity defect, that defect can be readily suppressed by light-mediated recruitment of Cdc24 to the plasma membrane (Figure 8). This result indicates that in the absence of polymerized actin, Cdc42 still associates with the plasma membrane. Thus, actin filaments are more likely to promote, either directly or indirectly, the localization of the Cla4-Bem1-Cdc24 complex in a subset of cells.

Cell cycle regulation of Bem1/Cdc24 complex assembly

Although recruitment of either Bem1 or Cdc24 efficiently biases the site of polarization, at certain stages of the cell cycle the molecular consequences of their recruitment are quite distinct. In late G1, following commitment to the cell cycle, light-induced recruitment of either Bem1 or Cdc24 promotes accumulation of active Cdc42, endogenous Bem1, and cytosolic Cdc24 (Figure 2 and Figures 3 and 6, respectively). These results confirm prior models for polarization during the interval between Start and bud emergence. However, Bem1 recruitment does not affect the kinetics of Cdc42 activation, Cdc24 accumulation, or endogenous Bem1 accumulation. In contrast, optogenetic recruitment of the GEF Cdc24 induces precocious

activation of Cdc42 and accumulation of cytosolic Cdc24, though neither are sufficient to induce accumulation of endogenous Bem1 prior to Cdk1 activation (Figures 3 and 5, respectively). Collectively, these results indicate that Cdk1 regulates the Bem1-Cdc24 complex; and, as a consequence of this regulation, previous models do not apply to the period prior to Start. Rather, a second mode of positive feedback operates in this interval.

Consistent with that interpretation, we find that Cdc24, Bem1, and Cdc42-GTP do not invariably colocalize, with the lowest level of colocalization occurring prior to Cdk1 activation (Figure 4). The delay in Bem1-dependent positive feedback relative to Whi5 nuclear exit (Figure 5) suggests that the polarity complex is regulated by Cln1/2 (Skotheim et al. 2008). We propose that Cdk1 activity promotes assembly of the Bem1-Cdc24 complex, which is consistent with the accumulation of Bem1 at the bud neck in early G1 without accompanying Cdc42 activation (Atkins et al. 2013) (Figure 4), as well as a Cln2-dependent increase in exchange activity towards Cdc42 (Howell et al. 2009).

Cdk1 activity may regulate the association of both Cdc24 with Bem1 and Bem1 with Cla4. If the former were constitutive, then Bem1 recruitment during early G1 should also result in Cdc24 recruitment which would induce Cdc42 activation (Figure 10). However, Bem1 recruitment in early G1 had no detectable effect on Cdc42 activation. Likewise, if the latter was constitutive, Cdc42 activation during G1 should induce Cla4 recruitment which would be predicted to induce Bem1 recruitment. However, Cdc42 recruitment in early G1 results in Cdc42 activation but does not result in Bem1 recruitment. These results suggest that the canonical polarity complex is not assembled prior to Start. G1 CDK activity is implicated in directly down regulating Rga2, a GTPase activating protein that plays a role in Cdc42 regulation (Sopko et al. 2007). CDK activation at start may therefore promote Cdc42 activation by at least two parallel pathways.

There also appears to be regulation of the positive feedback pathway after bud emergence. In polarized cells, Cdc24 recruitment at high light doses - but not Bem1 recruitment - activates

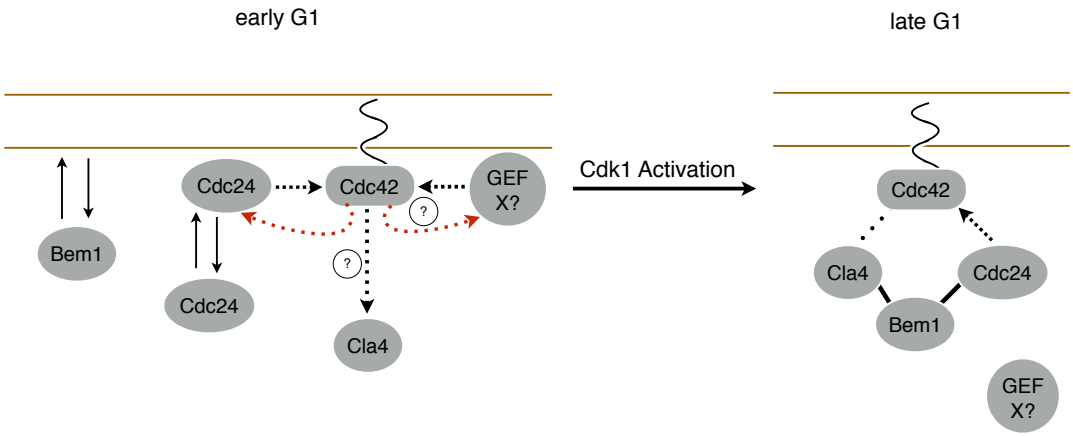

Figure 10: Model for polarity establishment.
In early G1, prior to Cdk1 activation, Cdc24, Bem1, and activated Cdc42 individually associate with the plasma membrane, but do not form stable complexes. With some frequency, Cdc24, and perhaps other Cdc42 GEFs, activate Cdc42 which can participate in a weak positive feedback loop with one or both GEFs. It is unclear whether Cdc42-GTP in early G1 interact with downstream effectors, such as Cla4, but if it does, it does not initiation Bem1 dependent positive feedback. Following Cdk1 activation, the Cla4-Bem1-Cdc24 complex assembles in late G1. This complex, may amplify the preexisting focus of Cdc42-GTP, and ultimately undergo strong positive feedback to generate a single focus of Cdc42-GTP that subsequently triggers bud emergence.

Cdc42, raising the possibility that the well studied Cdc24-Bem1-Cla4 complex functions as a unit for a limited fraction of the cell cycle surrounding polarization.

Coordination between Cdc42 activation before and after Start

What could be the function of the secondary positive feedback resulting in Cdc42 activity before Start? Current models suggest that Cdc42 activation initiates upon Cdk1 activation (Howell and Lew 2012). According to this model, stochastic activation of Cdc42 recruits the Cla4-Bem1-Cdc24 complex which amplifies this local inhomogeneity through positive feedback. Alternatively, polarization may be initiated by local association of Cla4-Bem1-Cdc24 via any of its myriad membrane association motifs. Indeed, our results show that local recruitment of members of this complex is indeed sufficient to induce symmetry breaking polarization and override the endogenous Rsr1 pathway. However, because Cdc24 can activate Cdc42 prior to Start, and because active Cdc42 is detected prior to Start (Figure 4), the site of polarization may not be dictated strictly by molecular noise or stochastic encounters of the Bem1-Cla4-Cdc24 complex with the membrane. Rather, a distinct mechanism(s) may exist that seeds the cortex with activated pools of Cdc42 during early G1 which pattern the “random” choice of bud site

upon passage through Start (Figure 10). The linking of two mechanisms for Cdc42 activation could allow for more rapid axis specification than could be achieved by a reaction-diffusion based mechanism alone (Goryachev and Pokhilko 2008). Indeed, such linked systems have been observed and modeled in a manner that can account for the speed of polarization events such as cell migration and the fixation of a single axis following an exploratory phase capable of reorientation (Brandman et al. 2005; Xiong et al. 2010).

Competition enforces singularity

Wild-type yeast cells rarely form multiple buds in a single cell cycle, suggesting the existence of mechanisms by which nascent bud sites compete in a winner take all competition. Recent work has shown that prior to bud emergence, cells are capable of forming multiple nascent foci. Yet, by employing mechanism(s) that appear to involve negative feedback, only one focus matures into the site of polarization (Howell et al. 2012), indicating competition between the nascent foci. Cells have been genetically manipulated to generate multiple buds. For example, expression of activated alleles of Cdc42 can induce the formation of multiple buds (Caviston, Tcheperegine, and Bi 2002). Similarly, multiple buds result from membrane-tethering either Bem1 or a Cdc24 mutant that is resistant to negative feedback, while also hindering the membrane-cytoplasm exchange of Cdc42 by deleting the facilitating chaperone, Rdi1. (Wu et al. 2015). However, despite the fact that transient optogenetic membrane recruitment of Bem1 or Cdc24 can induce efficient polarization, neither proved robust enough to generate two buds, indicating that the competition mechanism(s) are sufficiently strong to extinguish multiple nascent sites so that only a single axis emerges the winner. Two sites containing active Cdc42 could be generated, but we did not detect Bem1 at two sites simultaneously, consistent with models in which the intact Cla4-Bem1-Cdc24 complex is tightly limited (Wu et al. 2015).

Nascent sites also compete during early G1, prior to Start. Whereas a pool of Cdc42 can be induced in early G1 and maintained, if Cdc24 is recruited to a new site within the cell, the pool of

active Cdc42 at the original site dissipates within a few minutes in response to the new site (Figure 7). As these sites appear to be Bem1 deficient, this suggests that a distinct mechanism of competition is active during this time. Indeed, whereas optogenetic recruitment of Cdc24 can induce two sites of Cdc42 activation during G1 that can co-exist, once Cdk1 is activated, the competition is more stringent and Bem1 only accumulates to detectable levels at one of the two sites.

Optogenetics in dissection of cellular processes

In this study we show the utility of optogenetics in dissecting cellular processes. The ability to control the spatiotemporal dynamics of signaling molecules allows novel perturbations of cells that can lead to new insights. By exogenously localizing a GEF, we find that yeast cells are capable of activating Cdc42 just after mitotic exit. We also uncovered a cell cycle regulated step in polarity establishment: activation of the canonical positive feedback loop by Cdk1 (Figure 5 and Figure 6). Furthermore, we discovered a second positive feedback loop that functions independently of the canonical positive feedback mechanism and is active prior to Cdk1 activation (Figure 6). Finally, because optogenetics allows proteins to be dynamically repositioned in one or more spots we found that yeast cells are remarkably resistant to formation of multiple sites of polarization.

Methods

Plasmid and strain construction

DNA manipulations were simulated with SnapGene (GSL Biotech). Plasmids were generated using a combination of conventional ligation, homologous recombination (SLICE) in bacteria (Zhang, Werling, and Edelmann 2012), and Gibson Assembly (Gibson et al. 2009). All plasmids were verified by DNA sequencing.

All strains were constructed in the W303 background (leu2- 3 112 ura3-52 can1-100 ade2-1 his3-11 trp1-1). Haploid a and α cells were mated by incubating overnight in 500 μL YPD and then plating on selective media. All integrating plasmids were of the YIplac series. All low copy plasmids were of the pRS series (Supplemental Material Table S2). Gene deletions were generated by one-step gene disruptions using standard procedure. Yeast were transformed using lithium acetate, single-stranded carrier DNA and polyethylene glycol. All strains were verified by colony PCR. Endogenous genes were epitope tagged by one-step PCR (Longtine et al. 1998). PCR products for C-terminal td-Tomato fusions were amplified from a plasmid containing a tdTomato::HIS3MX cassette (DLB3299, a generous gift from Danny Lew). The endogenous Cdc24 promoter sequence consisted of 600bp upstream of the *cdc24* locus that was amplified from genomic DNA and inserted by Gibson Assembly into Cen plasmids that encoded for either Cdc24-GFP or Cdc24-tdTomato.

The *cdc28-as1* allele was inserted by linearizing a hygromycin-resistant plasmid containing the *cdc28-as1* coding sequence with an AflII restriction enzyme site adjacent to the F88G point mutation (pKW50); the plasmid encoding the *cdc28-as1* allele was generously provided by Eric Weiss (pELW886).

Treatment of cells for live cell imaging and drug treatment

Cells were grown in the dark at room temperature overnight in SC -His-Leu-Ura-Trp+Ade and diluted to OD600 = 0.1-0.2. For optogenetic experiments, cells were treated with 50 nM of ß-

estradiol after 2 hours of growth to induce expression of the optogenetic components. After 2 hours of induction, cells were concentrated 10-fold to 20-fold in fresh media + ß-estradiol and prepped for imaging. Cells co-expressing Cdc24-tdTomato and Cdc24-ePDZ, were induced for 90 minutes to limit deleterious overexpression of the GEF. For experiments less than 2 hours, cells were imaged on a 2.5% agar pad soaked in minimal media + ß-estradiol + drug (where applicable) for > 20 minutes. For experiments longer than 2 hours, cells were imaged in a CellASIC Onix microfluidic perfusion chamber (EMD Millipore Corporation) to provide continuous nutrients. For non-optogenetic experiments, cells were concentrated 10-fold to 20-fold after 2 hours of growth and imaged on 2.5% agar pad soaked in minimal media.

After 1.5 hours of induction with 50 nM ß-estradiol, *cdk1-as* cells were treated with 75 μM 1NM-PP1 or solvent (1% DMSO) at room temperature, in the dark, and without shaking for 20 minutes. Subsequently, cells were imaged for > 90 minutes, for a total time in 1NM-PP1 of approximately 2 hours.

To synchronize diploid cells in early G1, exponentially growing cells were treated with 15 μg/ml nocodazole for 2 hours. Cells were induced with 50 nM ß-estradiol and treated with a second dose of nocodazole at 7.5 μg/ml. After 1 hour, cells were washed three times with fresh media and released into minimal media + 50nM ß-estradiol for 30 minutes. Cells were treated with 100 μM Latrunculin A (Molecular Probes) or solvent (1% ethanol) for 20 minutes and then imaged for 90 minutes.

Optogenetic manipulations

Cells were imaged on an Axiovert 200M microscope (Zeiss) equipped with a spinning disk confocal (CSU10, Yokogawa), a 20- mW, 561-nm laser (Cobolt), and an electron-multiplying charge-coupled device (EMCCD) camera (Cascade 512B, Photometrics) using a 63×, 1.4 numerical aperture objective (Zeiss). The microscope was controlled using MetaMorph (Molecular Devices). A 550-nm long-pass filter (Edmund Optics) was placed in the transmitted

light path to avoid photoexciting the LOV domain when using Nomarski optics. A galvanometer-steerable 440-nm dye laser (Micropoint, Photonics Instruments) for local photo excitation of Mid2-localized LOVpep. Illumination intensity was controlled by using an adjustable internal attenuator plate and an external optical density of 1.0 absorptive neutral density filter (ThorLabs) was placed in the beam path.

For polarization experiments, cells were photo-excited using the Micropoint laser. The coordinates of targeted sites (x, y, t) were recorded with each photo-excitation. Following illumination, a confocal tdTomato image and phase contrast image were acquired. For control (dark state) experiments, the experiment was performed identically except that the Micropoint laser was off. Exposure times were 500 msec for tdTomato and 100 msec for phase contrast.

Live cell imaging of unperturbed cells

For non-optogenetic experiments, cells were imaged with a Zeiss Axioimager M1 equipped with a Yokogawa CSU-X1 spinning disk unit (Solamere) and illuminated with 50-mW, 488-nm and 50-mW, 561-nm lasers (Coherent). Images were captured on a Cascade 1K electron microscope (EM) CCD camera or a Cascade 512BT (Photometrics) controlled by MetaMorph (Molecular Devices).

For maximum intensity Z-projection snapshots, cells were imaged through the center 3μm at 0.25μm slices. The GFP and tdTomato images were acquired sequentially, followed by a phase contrast image. Max intensity projections were generated using Metamorph. Single plane snapshots were acquired at the mid-plane of the cell, with GFP and tdTomato images acquired sequentially. Exposure times were 900 msec for tdTomato, 900 msec for GFP, and 66 msec for phase contrast.

Time-lapse imaging acquired single plane snapshots of a confocal tdTomato image and phase contrast image at the mid-plane of the cell. Cells were imaged at a rate of once per minute for 3 minutes, followed by a rate of once per 30 seconds for 4 minutes, and finally imaged at a rate of

once per minute for 3 minutes. Exposure times were 700 msec for tdTomato and 66 msec for phase contrast.

Image analysis

All images were analyzed in ImageJ (Schneider, Rasband, and Eliceiri 2012), with custom-written macros. To determine the angle between the laser position and the nascent bud site, we generated kymographs displaying the laser position, the site of bud emergence, and the intensity of the probe. To generate the kymographs, the cell outline was tracked using the plugin JFilament (Smith et al. 2010), which created a series of XY-coordinates to be converted into an ROI for each image in the stack . The ROI was then overlaid on its cognate image, linearized, and normalized to 100 pixels in length by 6 pixels in width. This was repeated iteratively through each slice of the stack to form a kymograph. The kymographs were annotated with the center coordinate of each target in each frame of the time-lapse, the time and position of bud emergence, and the position of the previous bud site.

Polarization Efficiency was defined as $(1-2\theta/\pi)$ where θ is the angle between the site of illumination and the position of the nascent bud. A population measure of polarization efficiency was found by taking the average of the polarization efficiency value for all cells.

To quantify the appearance time of a polarity component, the time of bud emergence, and the polarization efficiency, we analyzed time-lapse images as follows: cells were only scored if they underwent both polarization and bud emergence within the time-course of the movie. The analysis was limited to mother cells and cells that budded within the first 20 minutes were excluded. In cells in which Whi5 nuclear exit was scored, nuclear exit was defined as when nuclear Whi5 signal equaled that of the cytoplasm. To quantify the appearance of weak fluorescent signals, accumulation was scored by blinding the fluorescent image and scoring manually, by eye, accumulation of the probe.

To analyze colocalization, cells were separated into cell cycle stages depending on both the bud size and the distribution of the probes. Data were blinded and cells were pulled at random from each cell cycle subset. The number of puncta with colocalization (GFP with tdTomato and tdTomato with GP) was manually counted.

For *cdk1-as* cells, we limited our analysis to large-budded mother cells that accumulated Bem1 or the Cdc42 biosensor to the bud neck, indicative of early G1 cells. A "large-bud" was considered to have an area more than 4.5 μm^2. As *cdk1-as* cells treated with 1NM-PP1 do not undergo bud emergence, to be scored as polarized, they needed to maintain polarization for >15 minutes.

To quantify competition in dynamic reorientation experiments, a targeting event was scored as "Outcompeted" if the Cdc42 biosensor signal disappeared from the initial position and accumulated at the new position within the time that the target was maintained at the new position. The event was deemed "Not Outcompeted" if the Cdc42 biosensor neither disappeared from the initial position nor accumulated at the new position.

Acknowledgments

This work was supported by NIH R01GM85087. KW was funded (in part) by NIH T32 GM007183, and D.S. was supported by an American Cancer Society Postdoctoral Fellowship (119248-PF-10-134-01-CCG). We thank Eric Weiss and Danny Lew for generous gifts of reagents and Ed Munro, Mike Rust, Dave Kovar, Danny Lew, and members of the Glotzer lab for helpful discussions and support.

Literature Cited

Atkins, B D, S Yoshida, K Saito, C F Wu, Daniel J Lew, and D Pellman. 2013. "Inhibition of Cdc42 During Mitotic Exit Is Required for Cytokinesis." *The Journal of Cell Biology* 202 (2): 231–40. doi:10.1083/jcb.201301090.

Bishop, A C, J A Ubersax, D T Petsch, D P Matheos, N S Gray, J Blethrow, E Shimizu, et al. 2000. "A Chemical Switch for Inhibitor-Sensitive Alleles of Any Protein Kinase.." *Nature* 407 (6802): 395–401. doi:10.1038/35030148.

Bose, I, J E Irazoqui, J J Moskow, E S Bardes, T R Zyla, and Daniel J Lew. 2001. "Assembly of Scaffold-Mediated Complexes Containing Cdc42p, the Exchange Factor Cdc24p, and the Effector Cla4p Required for Cell Cycle-Regulated Phosphorylation of Cdc24p.." *The Journal of Biological Chemistry* 276 (10): 7176–86. doi:10.1074/jbc.M010546200.

Brandman, Onn, James E Ferrell, Rong Li, and Tobias Meyer. 2005. "Interlinked Fast and Slow Positive Feedback Loops Drive Reliable Cell Decisions.." *Science (New York, N.Y.)* 310 (5747): 496–98. doi:10.1126/science.1113834.

Butty, Anne-Christine, Nathalie Perrinjaquet, Audrey Petit, Malika Jaquenoud, Jeffrey E Segall, Kay Hofmann, Catherine Zwahlen, and Matthias Peter. 2002. "A Positive Feedback Loop Stabilizes the Guanine-Nucleotide Exchange Factor Cdc24 at Sites of Polarization.." *The EMBO Journal* 21 (7): 1565–76. doi:10.1093/emboj/21.7.1565.

Caviston, Juliane P, Serguei E Tcheperegine, and Erfei Bi. 2002. "Singularity in Budding: a Role for the Evolutionarily Conserved Small GTPase Cdc42p.." *Proc Natl Acad Sci U S A* 99 (19): 12185–90. doi:10.1073/pnas.182370299.

Chenevert, J, K Corrado, A Bender, J Pringle, and I Herskowitz. 1992. "A Yeast Gene (BEM1) Necessary for Cell Polarization Whose Product Contains Two SH3 Domains.." *Nature* 356 (6364): 77–79. doi:10.1038/356077a0.

Costanzo, Michael, Joy L Nishikawa, Xiaojing Tang, Jonathan S Millman, Oliver Schub, Kevin Breitkreuz, Danielle Dewar, Ivan Rupes, Brenda Andrews, and Mike Tyers. 2004. "CDK Activity Antagonizes Whi5, an Inhibitor of G1/S Transcription in Yeast.." *Cell* 117 (7): 899–913. doi:10.1016/j.cell.2004.05.024.

Etienne-Manneville, Sandrine. 2004. "Cdc42--the Centre of Polarity.." *Journal of Cell Science* 117 (Pt 8): 1291–1300. doi:10.1242/jcs.01115.

Freisinger, Tina, Ben Klünder, Jared Johnson, Nikola Müller, Garwin Pichler, Gisela Beck, Michael Costanzo, et al. 2013. "Establishment of a Robust Single Axis of Cell Polarity by Coupling Multiple Positive Feedback Loops." *Nature Communications* 4 (May): 1807. doi:10.1038/ncomms2795.

Gibson, Daniel G, Lei Young, Ray-Yuan Chuang, J Craig Venter, Clyde A Hutchison, and Hamilton O Smith. 2009. "Enzymatic Assembly of DNA Molecules Up to Several Hundred Kilobases.." *Nature Methods* 6 (5). Nature Publishing Group: 343–45. doi:10.1038/nmeth.1318.

Goryachev, Andrew B, and Alexandra V Pokhilko. 2008. "Dynamics of Cdc42 Network Embodies a Turing-Type Mechanism of Yeast Cell Polarity." *FEBS Letters* 582 (10): 1437–43. doi:10.1016/j.febslet.2008.03.029.

Holly, S P, and K J Blumer. 1999. "PAK-Family Kinases Regulate Cell and Actin Polarization Throughout the Cell Cycle of Saccharomyces Cerevisiae.." *The Journal of Cell Biology* 147 (4): 845–56.

Howell, Audrey S, and Daniel J Lew. 2012. "Morphogenesis and the Cell Cycle.." *Genetics* 190 (1): 51–77. doi:10.1534/genetics.111.128314.

Howell, Audrey S, Meng Jin, Chi-Fang Wu, Trevin R Zyla, Timothy C Elston, and Daniel J Lew. 2012. "Negative Feedback Enhances Robustness in the Yeast Polarity Establishment

Circuit.." *Cell* 149 (2): 322–33. doi:10.1016/j.cell.2012.03.012.

Howell, Audrey S, Natasha S Savage, Sam A Johnson, Indrani Bose, Allison W Wagner, Trevin R Zyla, H Frederik Nijhout, Michael C Reed, Andrew B Goryachev, and Daniel J Lew. 2009. "Singularity in Polarization: Rewiring Yeast Cells to Make Two Buds.." *Cell* 139 (4): 731–43. doi:10.1016/j.cell.2009.10.024.

Irazoqui, Javier E, Amy S Gladfelter, and Daniel J Lew. 2003. "Scaffold-Mediated Symmetry Breaking by Cdc42p.." *Nature Cell Biology* 5 (12): 1062–70. doi:10.1038/ncb1068.

Johnson, D I, and J R Pringle. 1990. "Molecular Characterization of CDC42, a Saccharomyces Cerevisiae Gene Involved in the Development of Cell Polarity.." *The Journal of Cell Biology* 111 (1): 143–52.

Jose, Mini, Sylvain Tollis, Deepak Nair, Jean-Baptiste Sibarita, and Derek McCusker. 2013. "Robust Polarity Establishment Occurs via an Endocytosis-Based Cortical Corralling Mechanism.." *The Journal of Cell Biology* 200 (4): 407–18. doi:10.1083/jcb.201206081.

Kozubowski, Lukasz, Koji Saito, Jayme M Johnson, Audrey S Howell, Trevin R Zyla, and Daniel J Lew. 2008. "Symmetry-Breaking Polarization Driven by a Cdc42p GEF-PAK Complex." *Current Biology* 18 (22): 1719–26. doi:10.1016/j.cub.2008.09.060.

Longtine, M S, A McKenzie, D J Demarini, N G Shah, A Wach, A Brachat, P Philippsen, and J R Pringle. 1998. "Additional Modules for Versatile and Economical PCR-Based Gene Deletion and Modification in Saccharomyces Cerevisiae.." *Yeast (Chichester, England)* 14 (10): 953–61. doi:10.1002/(SICI)1097-0061(199807)14:10<953::AID-YEA293>3.0.CO;2-U.

Louvion, J F, B Havaux-Copf, and D Picard. 1993. "Fusion of GAL4-VP16 to a Steroid-Binding Domain Provides a Tool for Gratuitous Induction of Galactose-Responsive Genes in Yeast.." *Gene* 131 (1): 129–34.

Macara, Ian G. 2004. "Parsing the Polarity Code.." *Nature Reviews Molecular Cell Biology* 5 (3): 220–31. doi:10.1038/nrm1332.

McCusker, Derek, Carilee Denison, Scott Anderson, Thea A Egelhofer, John R Yates, Steven P Gygi, and Douglas R Kellogg. 2007. "Cdk1 Coordinates Cell-Surface Growth with the Cell Cycle.." *Nature Cell Biology* 9 (5): 506–15. doi:10.1038/ncb1568.

Mionnet, Cyril, Stéphanie Bogliolo, and Robert A Arkowitz. 2008. "Oligomerization Regulates the Localization of Cdc24, the Cdc42 Activator in Saccharomyces Cerevisiae.." *The Journal of Biological Chemistry* 283 (25): 17515–30. doi:10.1074/jbc.M800305200.

Ozbudak, Ertugrul M, Attila Becskei, and Alexander Van Oudenaarden. 2005. "A System of Counteracting Feedback Loops Regulates Cdc42p Activity During Spontaneous Cell Polarization.." *Developmental Cell* 9 (4): 565–71. doi:10.1016/j.devcel.2005.08.014.

Rossman, Kent L, David K Worthylake, Jason T Snyder, David P Siderovski, Sharon L Campbell, and John Sondek. 2002. "A Crystallographic View of Interactions Between Dbs and Cdc42: PH Domain-Assisted Guanine Nucleotide Exchange." *The EMBO Journal* 21 (6): 1315–26. doi:10.1093/emboj/21.6.1315.

Schneider, Caroline A, Wayne S Rasband, and Kevin W Eliceiri. 2012. "NIH Image to ImageJ: 25 Years of Image Analysis.." *Nature Methods* 9 (7): 671–75.

Skotheim, Jan M, Stefano Di Talia, Eric D Siggia, and Frederick R Cross. 2008. "Positive Feedback of G1 Cyclins Ensures Coherent Cell Cycle Entry.." *Nature* 454 (7202): 291–96. doi:10.1038/nature07118.

Smith, Matthew B, Hongsheng Li, Tian Shen, Xiaolei Huang, Eddy Yusuf, and Dimitrios Vavylonis. 2010. "Segmentation and Tracking of Cytoskeletal Filaments Using Open Active Contours.." *Cytoskeleton (Hoboken, NJ)* 67 (11). John Wiley & Sons, Inc.: 693–705. doi:10.1002/cm.20481.

Sopko, Richelle, Dongqing Huang, Jeffrey C Smith, Daniel Figeys, and Brenda J Andrews. 2007. "Activation of the Cdc42p GTPase by Cyclin-Dependent Protein Kinases in Budding

Yeast.." *The EMBO Journal* 26 (21): 4487–4500. doi:10.1038/sj.emboj.7601847.

Strickland, Devin, Yuan Lin, Elizabeth Wagner, C Matthew Hope, Josiah Zayner, Chloe Antoniou, Tobin R Sosnick, Eric L Weiss, and Michael Glotzer. 2012. "TULIPs: Tunable, Light-Controlled Interacting Protein Tags for Cell Biology.." *Nature Methods* 9 (4): 379–84. doi:10.1038/nmeth.1904.

Thompson, Barry J. 2013. "Cell Polarity: Models and Mechanisms From Yeast, Worms and Flies.." *Development (Cambridge, England)* 140 (1): 13–21. doi:10.1242/dev.083634.

Tischer, Doug, and Orion D Weiner. 2014. "Illuminating Cell Signalling with Optogenetic Tools.." *Nature Reviews Molecular Cell Biology* 15 (8): 551–58. doi:10.1038/nrm3837.

Tong, Zongtian, Xiang-Dong Gao, Audrey S Howell, Indrani Bose, Daniel J Lew, and Erfei Bi. 2007. "Adjacent Positioning of Cellular Structures Enabled by a Cdc42 GTPase-Activating Protein-Mediated Zone of Inhibition.." *The Journal of Cell Biology* 179 (7): 1375–84. doi:10.1083/jcb.200705160.

Wagner, Elizabeth, and Michael Glotzer. 2016. "Local RhoA Activation Induces Cytokinetic Furrows Independent of Spindle Position and Cell Cycle Stage.." *The Journal of Cell Biology* 213 (6). Rockefeller Univ Press: 641–49. doi:10.1083/jcb.201603025.

Wedlich-Soldner, Roland, Steve Altschuler, Lani Wu, and Rong Li. 2003. "Spontaneous Cell Polarization Through Actomyosin-Based Delivery of the Cdc42 GTPase.." *Science (New York, N.Y.)* 299 (5610): 1231–35. doi:10.1126/science.1080944.

Woods, Benjamin, Chun-Chen Kuo, Chi-Fang Wu, Trevin R Zyla, and Daniel J Lew. 2015. "Polarity Establishment Requires Localized Activation of Cdc42.." *The Journal of Cell Biology* 211 (1): 19–26. doi:10.1083/jcb.201506108.

Wu, Chi-Fang, Jian-Geng Chiou, Maria Minakova, Benjamin Woods, Denis Tsygankov, Trevin R Zyla, Natasha S Savage, Timothy C Elston, and Daniel J Lew. 2015. "Role of Competition Between Polarity Sites in Establishing a Unique Front.." *eLife* 4: 399. doi:10.7554/eLife.11611.

Xiong, Yuan, Chuan-Hsiang Huang, Pablo A Iglesias, and Peter N Devreotes. 2010. "Cells Navigate with a Local-Excitation, Global-Inhibition-Biased Excitable Network.." *Proceedings of the National Academy of Sciences of the United States of America* 107 (40): 17079–86. doi:10.1073/pnas.1011271107.

Zhang, Yongwei, Uwe Werling, and Winfried Edelmann. 2012. "SLiCE: a Novel Bacterial Cell Extract-Based DNA Cloning Method.." *Nucleic Acids Research* 40 (8): e55. doi:10.1093/nar/gkr1288.

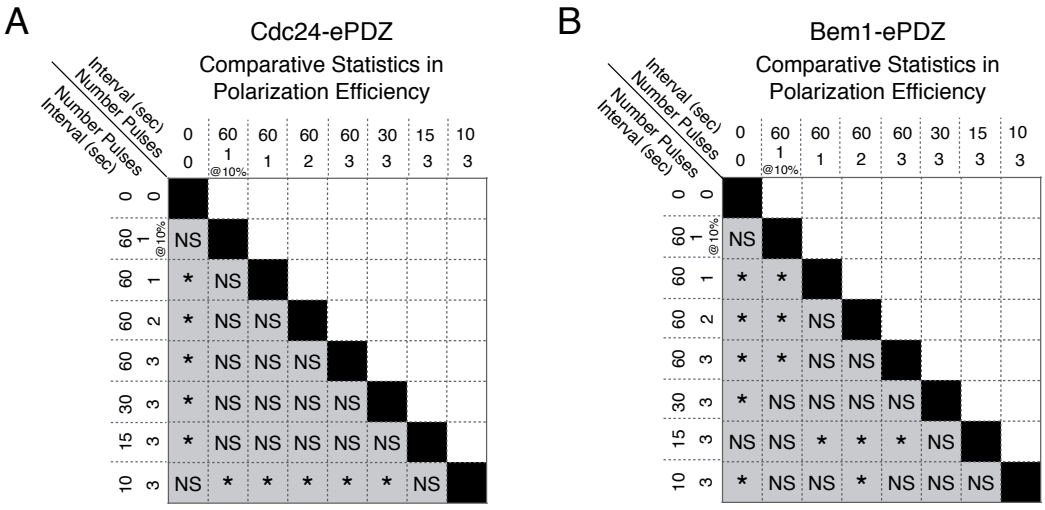

Figure 1- Supplemental Figure 1: Statistical analysis of polarization efficiency as a function of light dose (Figure 1D).

A) Comparative statistical analysis for polarization efficiency in response to Cdc24-ePDZ recruitment and light dose. NS indicates populations not statistically different at $p = 0.05$, * denotes statistically significant at $p < 0.05$, Mann-Whitney *U* test.

B) Comparative statistics for Polarization efficiency in response to increasing light dose and Bem1 recruitment as in **A**.

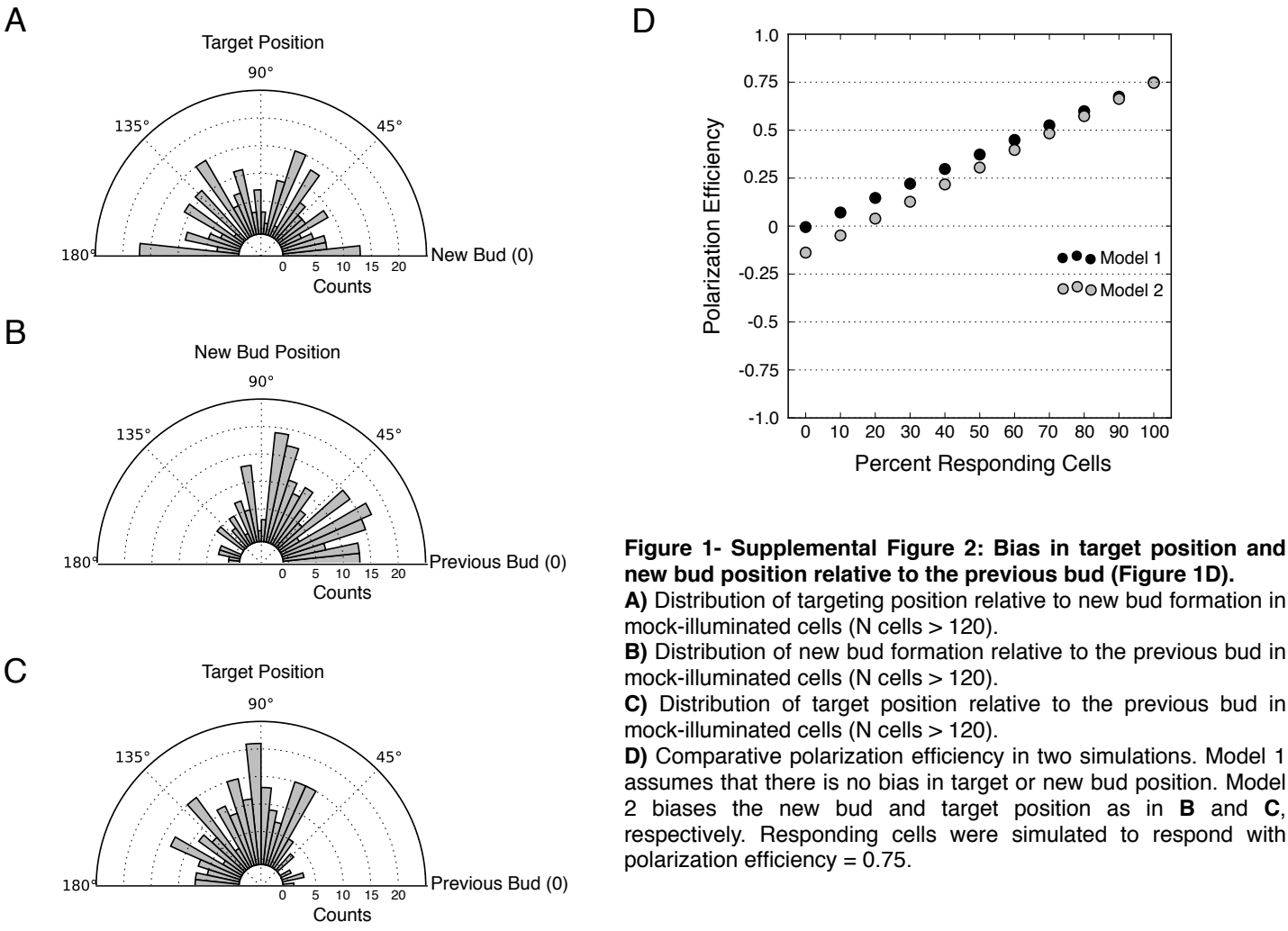

Figure 1- Supplemental Figure 2: Bias in target position and new bud position relative to the previous bud (Figure 1D).
A) Distribution of targeting position relative to new bud formation in mock-illuminated cells (N cells > 120).
B) Distribution of new bud formation relative to the previous bud in mock-illuminated cells (N cells > 120).
C) Distribution of target position relative to the previous bud in mock-illuminated cells (N cells > 120).
D) Comparative polarization efficiency in two simulations. Model 1 assumes that there is no bias in target or new bud position. Model 2 biases the new bud and target position as in **B** and **C**, respectively. Responding cells were simulated to respond with polarization efficiency = 0.75.

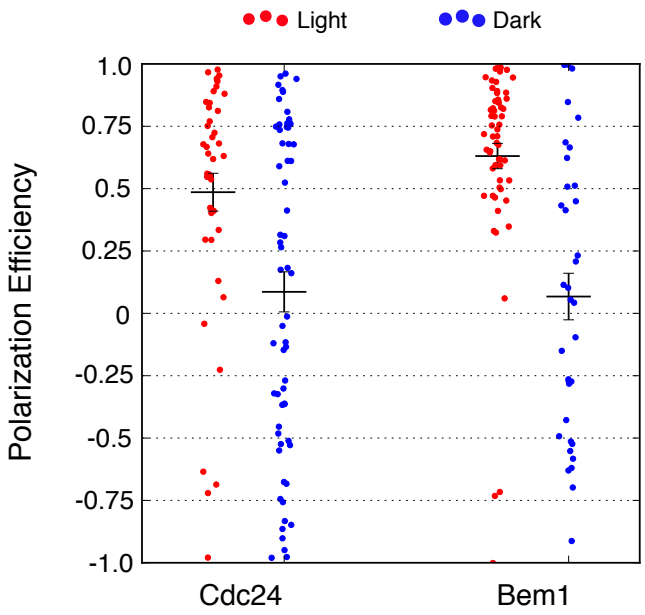

Figure 1- Supplemental Figure 3: Local accumulation of either Cdc24 or Bem1 is sufficient to override the endogenous Rsr1 pathway.
Polarization efficiency of a population of cells heterozygous for Rsr1. Each point represents an individual cell. Average and +/- SEM is indicated.

Figure 1- Supplemental Figure 4

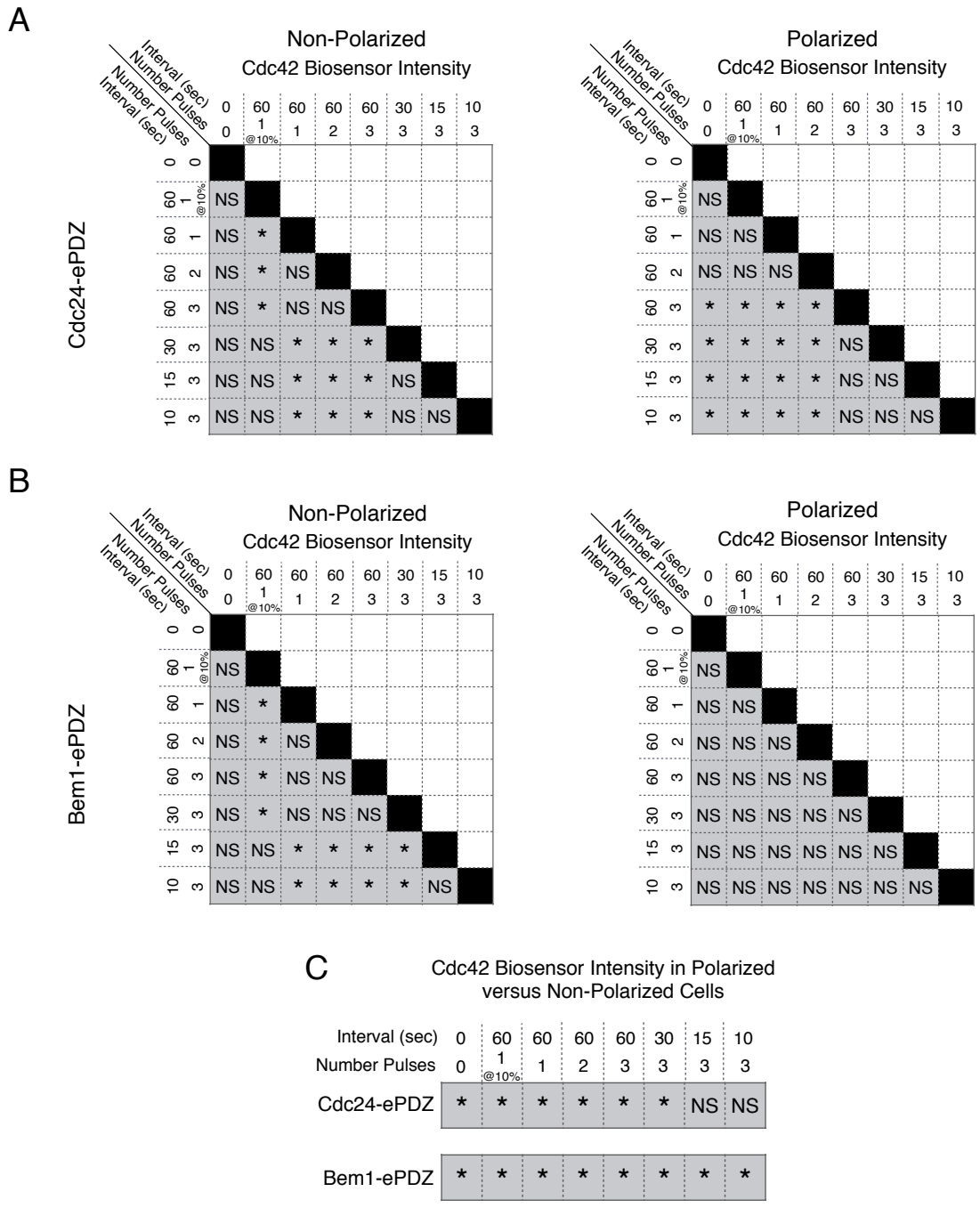

Figure 1- Supplemental Figure 4: Statistical analysis of Cdc42 biosensor accumulation in Polarized and Non-Polarized cells as a function of light dose (Figure 1F).

A) Statistical analysis for Cdc42 biosensor accumulation in response to Cdc24-ePDZ recruitment in polarized and non-polarized cells. NS indicates populations not statistically different at $p = 0.05$, * denotes statistically significant at $p < 0.05$, Mann-Whitney *U* test.

B) Statistics for Cdc42 biosensor accumulation in response to Bem1 recruitment as in **A**.

C) Statistical comparison of Cdc42 biosensor accumulation in polarized vs. non-polarized cells at each light dose. Statistical analysis as in **A** and **B**.

Figure 2 - Supplemental Figure 1

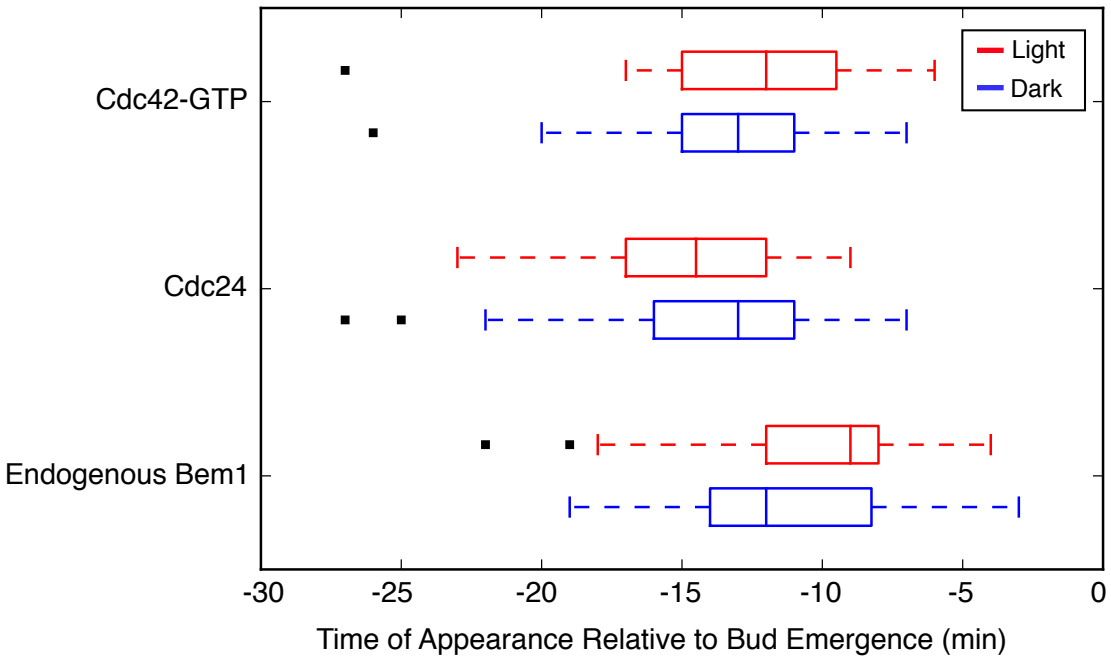

Figure 2 - Supplemental Figure 1: Photo-recruited Bem1 induces accumulation of Cdc42 biosensor, Cdc24, and Bem1
Box-and-whisker plot of Cdc42-GTP and Cdc24 appearance in response to Bem1 recruitment in photo-activated (red) or mock-illuminated (blue) cells. Outliers are depicted by black squares. Data are as in **Figure 3B**.

Figure 3 - Supplemental Figure 1

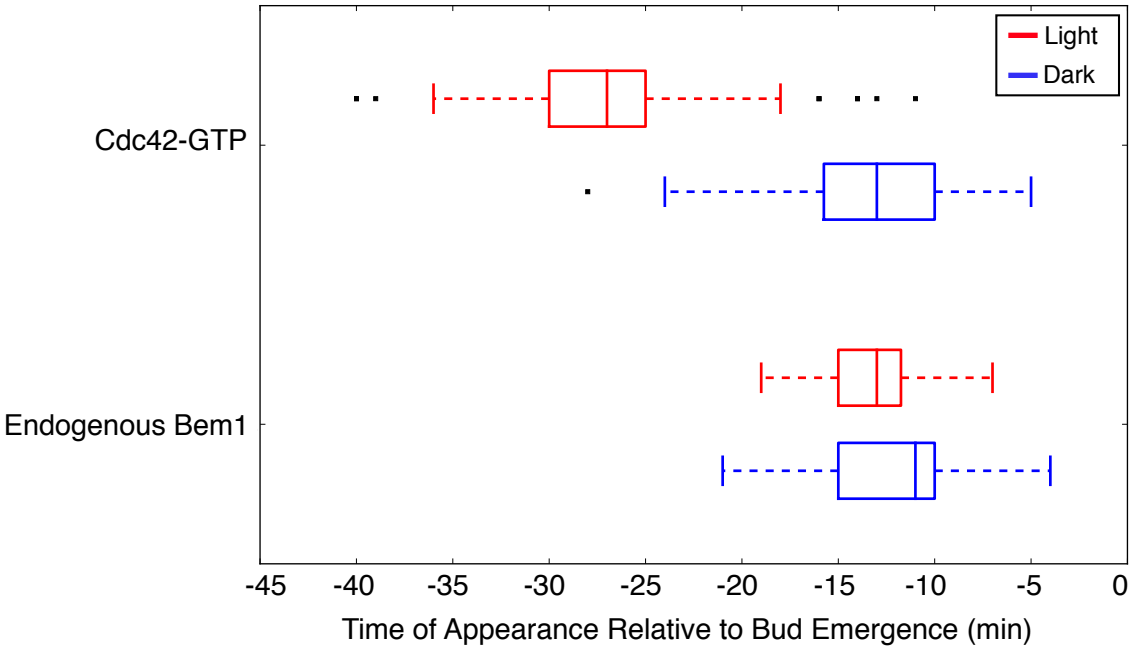

Figure 2 - Supplemental Figure 1: Light-induced recruitment of Cdc24 precociously activates Cdc42, but does not alter Bem1 kinetics.
Box-and-whisker plot of Cdc42-GTP and Bem1 appearance in photo-activated (red) and mock-illuminated (blue) cells. Outliers are depicted by black squares. Bud emergence occurs at time = 0. Data are as in **Figure 3D**.

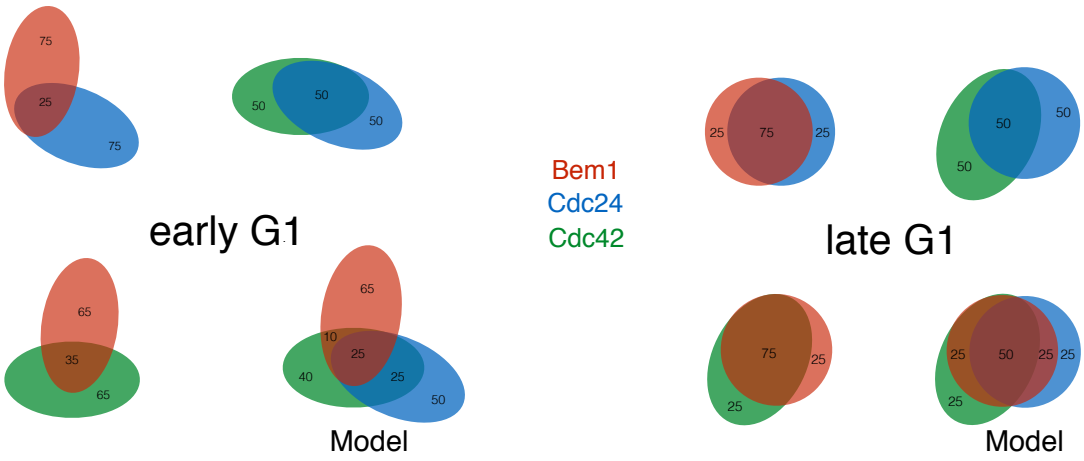

Figure 4 - Supplemental Figure 1: Pairwise analysis depicting the percent colocalization (related to Figure 4B). Venn diagrams for early G1 and late G1 depicting the extent of colocalization between each pair. The colocalization of all three components is presented in a model that is consistent with the pair-wise results. Data are as in **Figure 4B**.

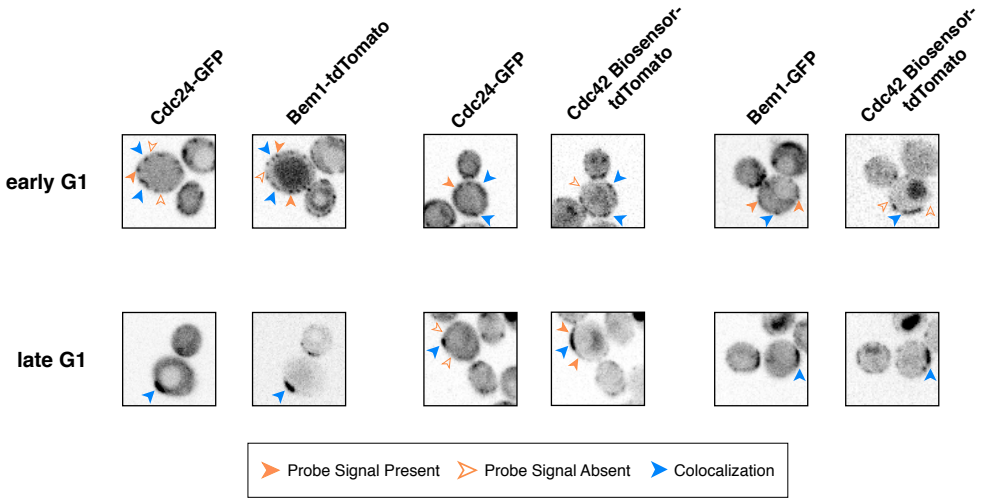

Figure 4 - Supplemental Figure 2: Single-plane images depict similar distributions as Z-stack projections. Single plane snapshots feature similar distributions of Cdc24, Bem1, and Cdc42-GTP.

Figure 5 - Supplemental Figure 1

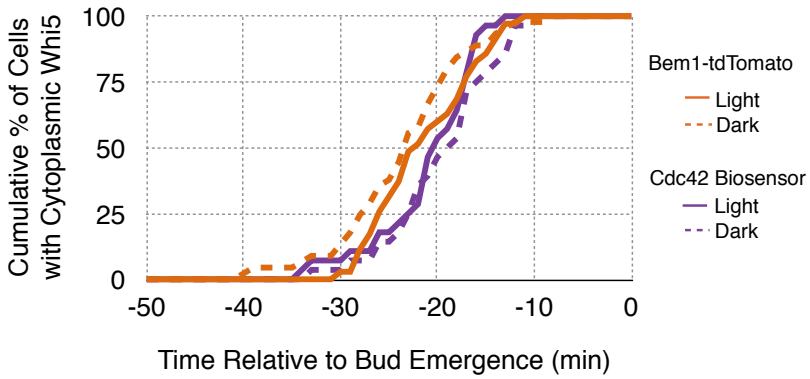

Figure 5 - Supplemental Figure 1: Expression of probe nor illumination affect the timing of Whi5 nuclear exit.
Nuclear exit timing for Whi5 for each condition in **Figure 5B** plotted on a single plot.

Figure 5 - Supplemental Figure 2

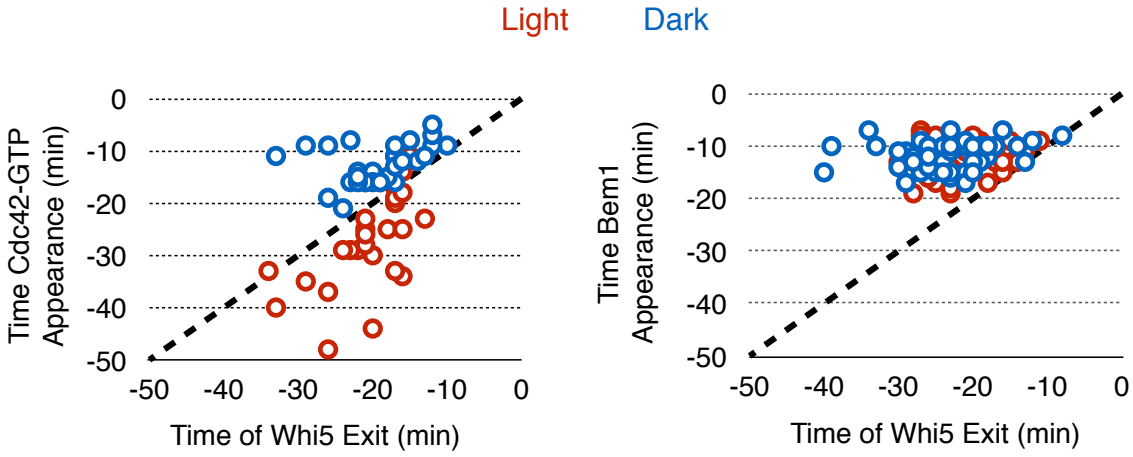

Figure 5 - Supplemental Figure 2: Photo-recruited Cdc24 activates Cdc42 prior to Whi5 nuclear exit.
Correlation between Whi5 nuclear exit and either Cdc42 activation or Bem1 accumulation at Cdc24 recruitment sites. Dashed line indicates the event and Whi5 nuclear exit occurring simultaneously. Points below the dashed line indicate the event occurs before Whi5 nuclear exit. Points above the line indicate the event occurs after Whi5 nuclear exit. Data are as in **Figure 5B**.

Figure 5 - Supplemental Figure 3

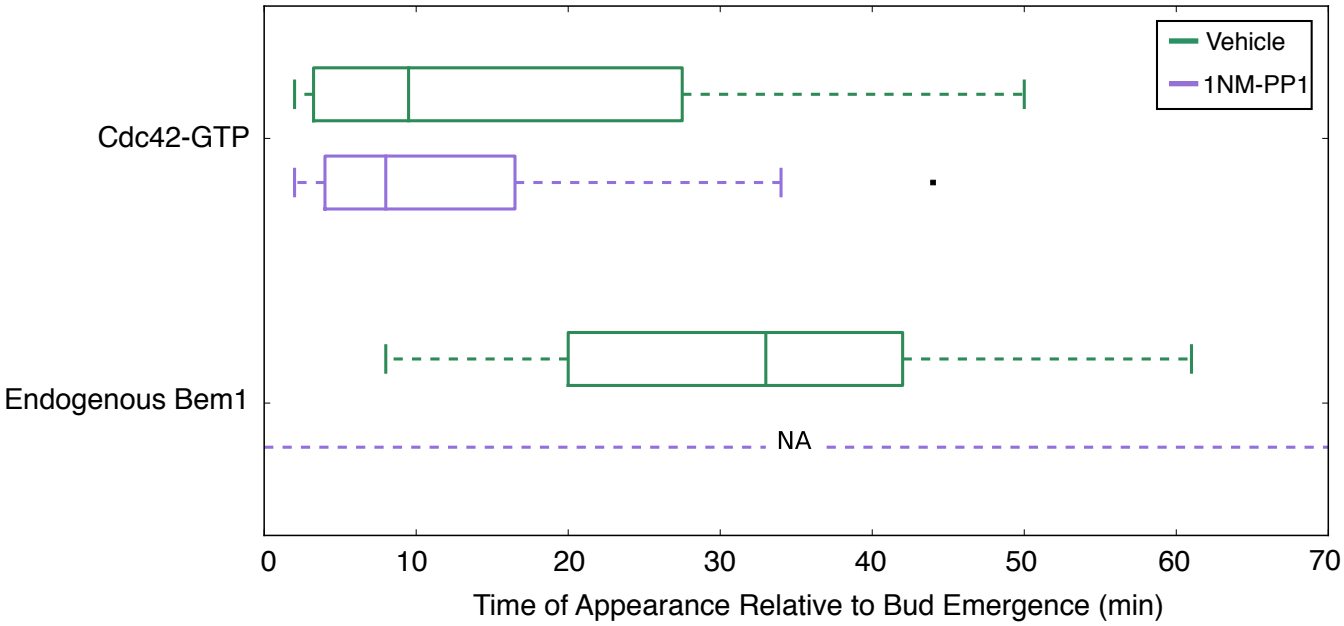

Figure 5 - Supplemental Figure 3: Bem1 accumulation requires Cdk1 activity in response to light-induced recruitment of Cdc24.
Box-and-whisker plot of Cdc42-GTP and Bem1 appearance in *cdk1-as* cells. Green boxes are vehicle-treated cells, while purple boxes are 1NM-PP1-treated cells. Outliers are depicted by black squares. Vehicle or 1NM-PP1 is added at time = -20 minutes; time = 0 is the start of live-cell imaging and photo-activation. Data are as in **Figure 3D**.

Figure 5 - Supplemental Figure 4

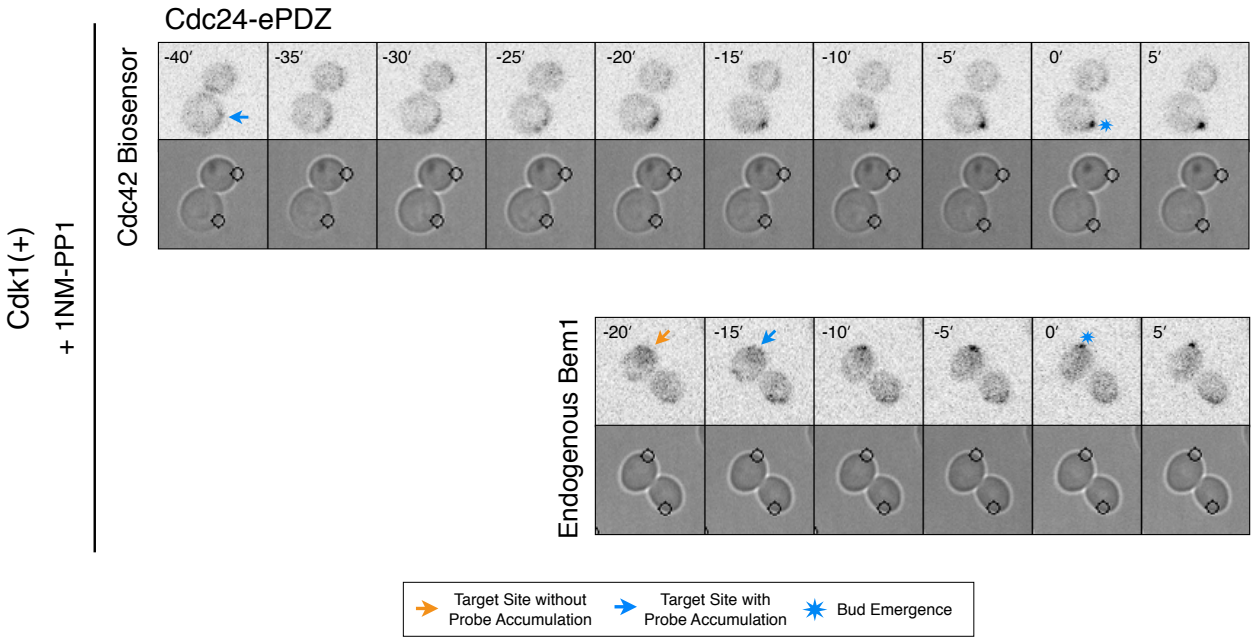

Figure 5 - Supplemental Figure 4: Addition of 1NM-PP1 to Cdk1(+) does not have adverse affects on Cdc42 biosensor or Bem1 accumulation or on bud emergence.
Fluorescent and phase images depicting representative Cdk1(+) treated with 1NM-PP1.

Figure 6 - Supplemental Figure 1

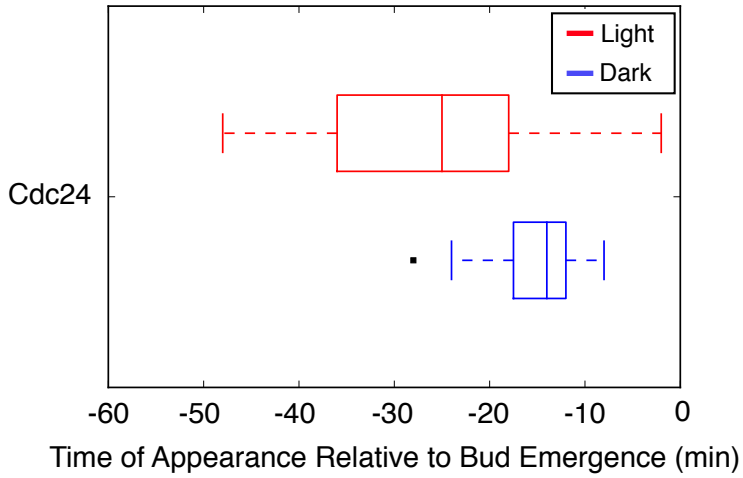

Figure 6 - Supplemental Figure 1: Optogenetic Cdc24 recruitment induces precocious accumulation of Cdc24-tdTomato.
Box-and-whisker plot of Cdc24-tdTomato appearance in photo-activated (red) and mock-illuminated (blue) cells. Outliers are depicted by black squares. Bud emergence occurs at time = 0. Data as in **Figure 6D.**

Figure 6 - Supplemental Figure 2

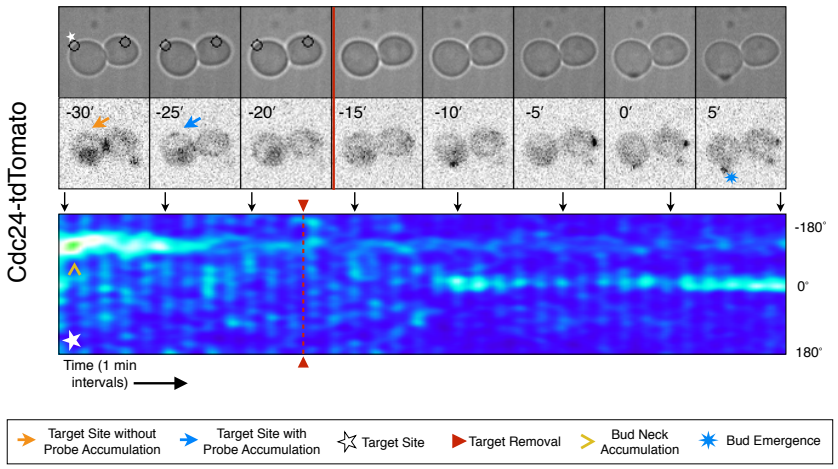

Figure 6 - Supplemental Figure 2: Transient Cdc24 recruitment can induce Cdc24-tdTomato accumulation, but cells can bud from an alternative position.
Representative fluorescence and phase time-course images for Cdc24-ePDZ transient recruitment when cells bud off target.

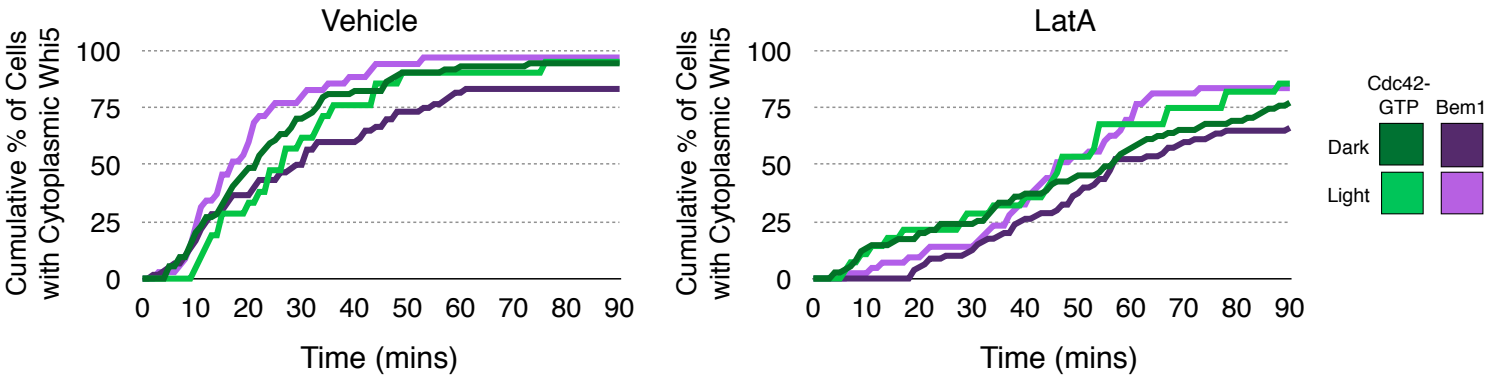

Figure 8 - Supplemental Figure 1: Loss of f-actin slows cell cycle entry.
Whi5 nuclear exit kinetics in Vehicle-treated (left) or LatrunculinA-treated (right) cells. Green lines refer to cells expressing the Cdc42 biosensor, while purple lines refer to cells expressing endogenous Bem1-tdTomato. Darker-colored lines represent mock-illuminated cells, while lighter-colored lines represent photo-activated cells (see schematic). Whi5 nuclear exit was slowed in LatA-treated cells. Data were binned by 5 minute intervals and combined across multiple experiments (n experiments = 2; N total cells > 40).

Table S1: Strain List

Strain	Genotype
WYK8301	TRP1Δ::Gal4-rMR1/+; pGal-pGal-Mid2-GFP-LOVpep::LEU/+/+; Bem1-tdTomato::HIS3MX/+; pGal-Cdc24-ePDZb1::URA/pADH1-Gal4-VP16-ER::URA; rsr1Δ::TRP1/rsr1Δ::KanMX
WYK8308	TRP1Δ::Gal4-rMR1/+; Gic2(1-208)-tdTomato::HIS3MX/+; pGal-Mid2-GFP-LOVpep::LEU/+; pGal-Bem1-ePDZb1::URA/pADH1-Gal4-VP16-ER::URA; rsr1Δ::TRP1/rsr1Δ::KanMX
WYK8318	TRP1Δ::Gal4-rMR1/+; Bem1-tdTomato::HIS3MX/+; pGal-Mid2-GFP-LOVpep::LEU/+; pGal-Bem1-ePDZb1::URA/pADH1-Gal4-VP16-ER::URA; rsr1Δ::TRP1/ rsr1Δ::KanMX
WYK8434	TRP1Δ::Gal4-rMR1/+; Gic2(1-208)-tdTomato::HIS3MX/+; pGal-Mid2-GFP-LOVpep::LEU/+; pGal-Bem1(R369A)-ePDZb1::URA/ pADH1-Gal4-VP16-ER::URA; rsr1Δ::TRP1/ rsr1Δ::KanMX
WYK8435	TRP1Δ::Gal4-rMR1/+; Gic2(1-208)-tdTomato::HIS3MX/+; pGal-Mid2-GFP-LOVpep::LEU/+; pGal-Bem1(P355A)-ePDZb1::URA/pADH1-Gal4-VP16-ER::URA; rsr1Δ::TRP1/ rsr1Δ::KanMX
WYK8436	TRP1Δ::Gal4-rMR1/+; Gic2(1-208)-tdTomato::HIS3MX/+; pGal-Mid2-GFP-LOVpep::LEU/+; pGal-Bem1(K482A)-ePDZb1::URA/pADH1-Gal4-VP16-ER::URA; rsr1Δ::TRP1/rsr1Δ::KanMX
WYK8437	TRP1Δ::Gal4-rMR1/+; Gic2(1-208)-tdTomato::HIS3MX/+; pGal-Mid2-GFP-LOVpep::LEU/+; pGal-Cdc24ΔPB1-ePDZb1::URA/pADH1-Gal4-VP16-ER::URA; rsr1Δ::TRP1/rsr1Δ::KanMX
WYK8439	TRP1Δ::Gal4-rMR1/+; Gic2(1-208)-tdTomato::HIS3MX/+; pGal-Mid2-GFP-LOVpep::LEU/+; pGal-Cdc24(Q412A R416E)-ePDZb1::URA/pADH1-Gal4-VP16-ER::URA; rsr1Δ::TRP1/rsr1Δ::KanMX
WYK8440	TRP1Δ::Gal4-rMR1/+; Gic2(1-208)-tdTomato::HIS3MX/+; pGal-Mid2-GFP-LOVpep::LEU/+; pGal-Cdc24-ePDZb1::URA/pADH1-Gal4-VP16-ER::URA; rsr1Δ::TRP1/rsr1Δ::KanMX
WYK8441	TRP1Δ::Gal4-rMR1/+; Bem1-tdTomato::HIS3MX/+; cdc28as::HygR/cdc28as::HygR; pGal-Mid2-GFP-LOVpep::LEU/+; pGal-Cdc24-ePDZb1::URA/pADH1-Gal4-VP16-ER::URA; rsr1Δ::TRP1/rsr1Δ::KanMX
WYK8442	TRP1Δ::Gal4-rMR1/+; Gic2(1-208)-tdTomato::HIS3MX/+; pGal-Mid2-GFP-LOVpep::LEU/+; cdc28as:HygR/cdc28as::HygR; pGal-Cdc24-ePDZb1::URA/pADH1-Gal4-VP16-ER::URA; rsr1Δ::TRP1/rsr1Δ::KanMX
WYK8500	TRP1Δ::Gal4-rMR1/+; Gic2(1-208)-tdTomato::HIS3MX/+; pGal-Mid2-GFP-LOVpep::LEU/+; pGal-Cdc24-ePDZb1::URA/pADH1-Gal4-VP16-ER::URA; Whi5-tdTomato:HIS3MX/+; rsr1Δ::TRP1/rsr1Δ::KanMX
WYK8502	TRP1Δ::Gal4-rMR1/+; pGal-Mid2-GFP-LOVpep::LEU/+; Bem1-tdTomato::HIS3MX/+; pGal-Cdc24-ePDZb1::URA/pADH1-Gal4-VP16-ER::URA; Whi5-tdTomato:HIS3MX/+; rsr1Δ::TRP1/rsr1Δ::KanMX
WYK8550	Bem1-GFP::HIS3MX/+; pADH1-Gal4-VP16-ER::URA/+; Gic2(1-208)-tdTomato::HIS3MX/+; rsr1Δ::TRP1/rsr1Δ::KanMX
WYK8551	TRP1Δ::Gal4-rMR1/+; Bem1-tdTomato::HIS3MX/+; pADH1-Gal4-VP16-ER::URA/+; pCdc24-Cdc24-GFP::LEU (pKW102); rsr1Δ::TRP/rsr1Δ::KanMX
WYK8552	pADH1-Gal4-VP16-ER::URA/+; Gic2(1-208)-tdTomato::HIS3MX/+; rsr1Δ::TRP/ rsr1Δ::KanMX; pCdc24-Cdc24-GFP::LEU (pKW102)
WYK8575	TRP1Δ::Gal4-rMR1/+; pGal-Mid2-GFP-LOVpep::LEU/+; pGal-Cdc24-ePDZb1::URA/ pADH1-Gal4-VP16-ER::URA; rsr1Δ::TRP1/rsr1Δ::KanMX; pCdc24-Cdc24-tdTomato::HIS3 (pKW101)
WYK8576	TRP1Δ::Gal4-rMR1/+; pGal-Mid2-GFP-LOVpep::LEU/+; pGal-Bem1-ePDZb1::URA/ pADH1-Gal4-VP16-ER::URA; rsr1Δ::TRP1/rsr1Δ::KanMX; pCdc24-Cdc24-tdTomato::HIS3 (pKW101)
WYK8598	TRP1Δ::Gal4-rMR1/+; pGal-Mid2-GFP-LOVpep::LEU/+; Gic2(1-208)-tdTomato::HIS3MX/+; pGal-Cdc24-ePDZb1::URA/pADH1-Gal4-VP16-ER::URA; rsr1Δ::KanMX/+
WYK8599	TRP1Δ::Gal4-rMR1/+; pGal-Mid2-GFP-LOVpep::LEU/+; Gic2(1-208)-tdTomato::HIS3MX/+; pGal-Bem1-ePDZb1::URA/pADH1-Gal4-VP16-ER::URA; rsr1Δ::KanMX/+
All strains are *MATa/MATα* diploids constructed in the W303 background. They have the following additional markers: *leu2-3,112 trp1-1 can1-100 ura3-1 ade2-1 his3-11,15*	

Table S2: Plasmid List

Plasmid Name	Type	Contents	Marker	Source
DLB3299	pFA6a	tdTomato	HIS3MX	Longtine *et al* 1998
pDS300	YIplac	pGal-Cdc24-ePDZb1	URA	Strickland *et al* 2012
pDS311	YIplac	pGal-Cdc24ΔPB1-ePDZb1	URA	This Study
pDS343	YIplac	pGal-Mid2-GFP-LOVpep250	LEU	This Study
pDS357	YIplac	pGal-Bem1-ePDZb1	URA	This Study
pDS377	YIplac	pGal-Bem1(R369A)-ePDZb1	URA	This Study
pDS381	YIplac	pGal-Bem1(P355A)-ePDZb1	URA	This Study
pDS382	YIplac	pGal-Bem1(K482A)-ePDZb1	URA	This Study
pKW34	YIplac	pGal-Cdc24(Q412A R416E)-ePDZb1	URA	This Study
pKW50	pFA6a	cdc28-as1	HygR	This Study
pKW101	pRS	pCdc24-Cdc24-tdTomato	HIS	This Study
pKW102	pRS	pCdc24-Cdc24-GFP	LEU	This Study
pELW886	pRS	cdc28-as1	URA	Bishop *et al* 2000
pELW909	YIplac	pADH1-Gal4-VP16-ER	URA	Louvion *et al* 1993

Figure Legends

Figure 1: Cdc24 can activate Cdc42 in both polarized and unpolarized cells.

A) The endogenous cue is mediated by a system involving Rsr1 to yield patterned budding. Rsr1 directly interacts with Bem1 and Cdc24 to recruit and activate Cdc42 at an adjacent bud position. Rsr1 recruits Bem1 and/or Cdc24 **(1)** to activate Cdc42 **(2)** adjacent to the previous bud neck. Cdc42 undergoes positive feedback **(3)** by interacting with Cla4 to promote its own accumulation.

B) In the absence of Rsr1, cells undergo a symmetry breaking event mediated by positive feedback. The symmetry breaking event may involve a stochastic accumulation of Cdc42-GTP at a unique location that then recruits the Cla4-Bem1-Cdc24 complex **(1)**. Cdc24 activates additional molecules of Cdc42 **(2)** to promote positive feedback **(3)**.

C) Light-induced symmetry breaking by recruiting the GEF Cdc24 to activate Cdc42 at a prescribed position and induce positive feedback. Localized photo-activation of LOVpep recruits Cdc24-ePDZb **(1)** to activate Cdc42 **(2)**. Activated Cdc42 interacts with Cla4 to induce positive feedback.

D) Polarization efficiency of a population of cells where each point represents an individual cell. The angle ɵ is defined by the angle between the site of bud emergence and the laser position. Data are averages of all cells across multiple experiments (n experiments > 2, N total cells > 25 for each group). Average and +/- SEM is indicated. Statistical analysis in Figure 1 - Supplemental Figure 1. Strains used: WYK8440 and WYK8301.

E) Representative phase and inverted fluorescent images depicting the activation of Cdc42 in response to either Cdc24 or Bem1 recruitment in polarized or non-polarized cells. Difference overlay images place the subtraction of the two fluorescent images overlaid onto the phase contrast image. An increase in fluorescent signal is depicted by red psuedo-coloring on the overlay. Cells were treated to increasing doses of light. Shown from bottom to top,

representative images for each group:1 pulse/60 sec, 3 pulses/30 sec, and 3 pulses/15 sec. Each image is 16.2 μm x 16.2 μm. Strains used: WYK8440 and WYK8301.

F) Box-and-Whisker plots depicting the relative change in mean fluorescence intensity of the Cdc42 biosensor at targeted regions. The relative intensity of polarized cells is the mean of the intensity at 10 minutes post initial illumination compared to the intensity prior to illumination. The relative intensity for non-polarized cells compares activation of the biosensor 10 minutes before bud emergence relative to the intensity prior to illumination. Data is combined across multiple experiments (n experiments > 2, N total cells > 25 for each group). Statistical analysis in Figure 1 - Supplemental Figure 3. Strains used: WYK8440 and WYK8301.

Figure 1- Supplemental Figure 1: Statistical analysis of polarization efficiency as a function of light dose (Figure 1D).

A) Comparative statistical analysis for polarization efficiency in response to Cdc24-ePDZ recruitment and light dose. NS indicates populations not statistically different at $p = 0.05$, * denotes statistically significant at $p < 0.05$, Mann-Whitney *U* test.

B) Comparative statistics for Polarization efficiency in response to increasing light dose and Bem1 recruitment as in **A**.

Figure 1- Supplemental Figure 2: Bias in target position and new bud position relative to the previous bud (Figure 1D).

A) Distribution of targeting position relative to new bud formation in mock-illuminated cells (N cells > 120).

B) Distribution of new bud formation relative to the previous bud in mock-illuminated cells (N cells > 120).

C) Distribution of target position relative to the previous bud in mock-illuminated cells (N cells > 120).

D) Comparative polarization efficiency in two simulations. Model 1 assumes that there is no bias in target or new bud position. Model 2 approximates the biases the new bud and target positions as in **B** and **C**, respectively. Specifically, responding cells were simulated to respond with polarization efficiency = 0.75. In model 1, cells that do not respond were assumed to bud randomly in the range 46°-180°, with an average angle of 90°, corresponding to the angle expected if both targets and the new bud were random relative to the previous bud. In Model 2, cells that do not respond were assumed to bud randomly in the range 46°-180°, with an average angle of 102°. as an average difference of 102° approximates the aggregate bias resulting from the experimental bias in target position and the bias in bud site selection (Figure 2 - Supplemental Figure 1).

Figure 1- Supplemental Figure 3: Local accumulation of either Cdc24 or Bem1 is sufficient to override the endogenous Rsr1 pathway

Polarization efficiency of a population of cells heterozygous for Rsr1. Each point represents an individual cell. Average and +/- SEM is indicated. Strains used: WYK8598 and WYK8599.

Figure 1- Supplemental Figure 4: Statistical analysis of Cdc42 biosensor accumulation in Polarized and Non-Polarized cells as a function of light dose (Figure 1F).

A) Statistical analysis for Cdc42 biosensor accumulation in response to Cdc24-ePDZ recruitment in polarized and non-polarized cells. NS indicates populations not statistically different at $p = 0.05$, * denotes statistically significant at $p < 0.05$, Mann-Whitney *U* test.

B) Statistics for Cdc42 biosensor accumulation in response to Bem1 recruitment as in **A**.

C) Statistical comparison of Cdc42 biosensor accumulation in polarized vs. non-polarized cells at each light dose. Statistical analysis as in **A** and **B**.

Figure 2: Local accumulation of Bem1 is sufficient to bias the bud site

A) Representative phase and fluorescence images and kymographs showing the position of the laser target and accumulation of the Cdc42 biosensor, Cdc24, and endogenous Bem1 (respectively). Each image is 16.2 μm x 16.2 μm. Kymographs are generated by iteratively linearizing the membrane at each time point (schematic). Bud emergence occurs at Y = 0° and at time = 0 minutes. Arrows between the kymograph and fluorescent images correlate to the time shown in the panels. Strains used: WYK8308, WYK8318, and WYK8576.

B) Accumulation kinetics for each component in response to Bem1 recruitment. Red line is photo-activated cells, blue line is mock-illuminated cells. Bud emergence is time = 0. Data combined across multiple experiments (n experiments > 2, N total cells > 30 for each condition).

C) Domain schematic of Bem1-ePDZ, with mutation sites and interactions.

D) Polarization efficiency of a population of cells as in **1F.** Red dots are single photo-activated cells. Blue dots are single mock-illuminated cells. Data is combined across multiple experiments (n experiments > 2, N total cells > 20 for each group). Error bars S.E.M. polarization efficiency of Bem1, Bem1 R369A, and Bem1 P355A in the light was statistically significant relative to Bem1 K482A light and dark, and their respective dark-state controls. Bem1 K482A was not statistically significant relative to its dark state control. $p < 0.05$, Mann-Whitney *U* test. Strains used: WYK8308, WYK8434, WYK8435, and WYK8436.

Figure 2 - Supplemental Figure 1. Photo-recruited Bem1 induces accumulation of Cdc42-GTP, Cdc24 and Bem1

Box-and-whisker plot of Cdc42-GTP and Cdc24 appearance in response to Bem1 recruitment in photo-activated (red) or mock-illuminated (blue) cells. Outliers are depicted by black squares. Data are as in **Figure 3B**.

Figure 3: Light-mediated recruitment of Cdc24 is sufficient to induce symmetry breaking

A) Domain schematic of Cdc24-ePDZ, with mutation sites and interactions.

B) Polarization efficiency of photo-illuminated (red) or mock-illuminated (blue) cells. Data are averaged across multiple experiments (n experiments > 2, N total cells > 20, for each group). Average and +/- S.E.M. indicated. polarization efficiency of Cdc24 and Cdc24ΔPB1 were statistically significant relative to Cdc24-GEF-dead light/dark, and statistically significant compared to their respective dark state controls. The difference between Cdc24 and Cdc24ΔPB1 were not statistically significant. The response to Cdc24-GEF dead was not statistically significant relative to its dark state control. $p < 0.05$, Mann-Whitney *U* test. Strains used: WYK8440, WYK8437, and WYK8439.

C) Panels of representative phase and fluorescence images and kymographs showing the position of the laser target and accumulation of a Cdc42 biosensor or endogenous Bem1 in response to Cdc24 recruitment. Each image is 16.2 μm x 16.2 μm. Strains used: WYK8440 and WYK8301.

D) Accumulation kinetics for the Cdc42 biosensor or endogenous Bem1 in response to Cdc24 recruitment. Data are combined across multiple experiments (n experiments > 2, N total cells > 30 for each condition).

Figure 3 - Supplemental Figure 1 Light-induced recruitment of Cdc24 precociously activates Cdc42, but does not alter Bem1 kinetics

Box-and-whisker plot of Cdc42-GTP and Bem1 appearance in photo-activated (red) and mock-illuminated (blue) cells. Outliers are depicted by black squares. Bud emergence occurs at time = 0. Data are as in **Figure 3D**.

Figure 4: Cdc42-GTP, Cdc24, and Bem1 do not constitutively colocalize and display rapid mobility prior to polarity establishment

A) Inverted fluorescent images depicting the three pairwise combinations of Cdc42-GTP, Bem1, and Cdc24. All images are Z projections of 0.25 μm slices for the center 3 μm. Each image is 13.5 μm x 13.5 μm. Strains used: WYK8550, WYK8551, and WYK8552.

B) Percentage of colocalization amongst puncta in early G1 or late G1 cells. Plots are separated by pairs as in **A**. Data are averages of all cells across multiple experiments (n experiments > 3; N cells > 20 for each condition; N total cells > 240). Error bars S.E.M. n.s indicates populations not statistically different at p >= 0.05, * p < 0.05, Mann-Whitney *U* test.

C) Time-lapse images capturing polarization in non-perturbed cells expressing either the Cdc42 Biosensor-tdTomato, endogenous Bem1-tdTomato, or Cdc24-tdTomato. Images are single planes of the center of the cell. Blue arrows denote the time and position of polarity establishment. Time = 0 is the onset of imaging, and images were captured for ten minutes at either 60 sec or 30 sec intervals as denoted. Strains used: WYK8301, WYK8440, and WYK8575.

Figure 4 - Supplemental Figure 1: Pairwise analysis depicting the percent colocalization (related to Figure 4B).

Venn diagrams for early G1 and late G1 depicting the extent of colocalization between each pair. The colocalization of all three components is presented in a model that is consistent with the pair-wise results. Data are as in **Figure 4B**.

Figure 4 - Supplemental Figure 2: Single-plane images depict similar distributions as Z-stack projections.

Single plane snapshots feature similar distributions of Cdc24, Bem1, and Cdc42-GTP. Each image is 13.5 μm x 13.5 μm. Strains used: WYK8550, WYK8551, and WYK8552.

Figure 5: Cdk1 Activation is required for Bem1 accumulation, but dispensable for Cdc42 activation

A) Representative panel of time-course images from Cdc24 recruitment in cells co-expressing Whi5-tdTomato with either the Cdc42 biosensor or Bem1-tdTomato. Each image is 16.2 μm x 16.2 μm. Strains used: WYK8500 and WYK8502.

B) Whi5 nuclear exit kinetics and accumulation kinetics for either Cdc42 activation or Bem1 at Cdc24 recruitment sites. Purple line represents Whi5 exit, with data combined for both light- and dark-state conditions as they are not significantly different (Figure 5 - Supplemental Figure 1). Bud emergence occurs at time = 0. Data are combined across multiple experiments (n experiments > 2; N total cells > 30 for each condition).

C) Representative panels and sub-images of cells depicting the response to Cdc24 recruitment +/- Cdk1 activity. Each inset is 6.5 μm x 6.5 μm. Strains used: WYK8441 and WYK8442.

D) Accumulation plots indicating the response of Cdc42 biosensor or Bem1 in response to Cdc24 recruitment +/- Cdk1 activity. Purple lines represent cells treated with 75 μM 1NM-PP1. Green lines represent Vehicle-treated cells. Data are combined across multiple experiments (n experiments = 2; N total cells > 40 for each condition).

Figure 5 - Supplemental Figure 1: Expression of probe nor illumination affect the timing of Whi5 nuclear exit.

Nuclear exit timing for Whi5 for each condition in **Figure 5B** plotted on a single plot.

Figure 5 - Supplemental Figure 2. Photo-recruited Cdc24 activates Cdc42 prior to Whi5 nuclear exit

Correlation between Whi5 nuclear exit and either Cdc42 activation or Bem1 accumulation at Cdc24 recruitment sites. Dashed line indicates the event and Whi5 nuclear exit occurring simultaneously. Points below the dashed line indicate the event occurs before Whi5 nuclear exit. Points above the line indicate the event occurs after Whi5 nuclear exit. Data are as in **Figure 5B**.

Figure 5 - Supplemental Figure 3. Bem1 accumulation requires Cdk1 activity in response to light-induced recruitment of Cdc24

Box-and-whisker plot of Cdc42-GTP and Bem1 appearance in *cdk1-as* cells. Green boxes are vehicle-treated cells, while purple boxes are 1NM-PP1-treated cells. Outliers are depicted by black squares. Vehicle or 1NM-PP1 is added at time = -20 minutes; time = 0 is the start of live-cell imaging and photo-activation. Data are as in **Figure 3D**.

Figure 5 - Supplemental Figure 4: Addition of 1NM-PP1 to Cdk1(+) does not have adverse affects on Cdc42 Biosensor or Bem1 accumulation or on bud emergence.

Fluorescent and phase images depicting representative Cdk1(+) treated with 1NM-PP1. Each image is 16.2 μm x 16.2 μm. Strains used: WYK8440 and WYK8301.

Figure 6: Cdc24 recruitment induces precocious Cdc42 activation and Cdc24-tdTomato accumulation that is self-sustaining

A) Phase and fluorescence images and kymographs of representative cells depicting the response to the transient recruitment of Cdc24-ePDZ or Bem1-ePDZ. Initial target site denoted by white stars. Each image is 16.2 μm x 16.2 μm. Strains used: WYK8440 and WYK8308.

B) Polarization efficiency following transient recruitment of Cdc24 and Bem1. Time indicates when the target was removed relative to bud emergence (bud emergence occurs at time = 0). Black dots represent polarization of individual cells in response to transient Cdc24 recruitment. Blue dots represent polarization of individual cells in response to transient Bem1 recruitment. Lines represent averages (+/- SEM) of data binned in 10 min intervals, with the middle time point represented on the plot. Results are pooled across multiple experiments (n experiments > 3; N cells > 10 for each time interval; N total cells > 75). Polarization Efficiencies of Cdc24 at -5, -15, and -25 min and Bem1 at -5 and -15 min were statistically significant relative to all earlier time points. Cdc24 and Bem1 Polarization Efficiencies were not statistically different at -45, -35, -15, and -5 min. $p < 0.05$, Mann-Whitney *U* test.

C) Representative phase and fluorescence images and kymographs showing the position of the laser target and accumulation of Cdc24-tdTomato in response to Cdc24-ePDZ recruitment. Strain used: WYK8575.

D) Accumulation kinetics for Cdc24-tdTomato. Data are combined across multiple experiments (n experiments > 2, N total cells > 30 for each condition).

E) Panels of representative phase and fluorescence images indicating the response of Cdc24-tdTomato to transient Cdc24-ePDZ recruitment. Orange arrows denote sites of illumination without Cdc24-tdTomato accumulation. Purple arrowhead indicates erroneous signal from vacuole. Strain used: WYK8575.

F) Stacked bar chart indicating the percentage of cells that maintain Cdc24-tdTomato accumulation in response to Cdc24 recruitment and whether they polarize to the prescribed site. Data is binned by 10 minute time intervals, with the middle time point represented on the plot.

Data combined across multiple experiments (n experiments > 3, N total cells > 25 for each condition).

Figure 6 - Supplemental Figure 1: Optogenetic Cdc24 recruitment induces precocious accumulation of Cdc24-tdTomato

Box-and-whisker plot of Cdc24-tdTomato appearance in photo-activated (red) and mock-illuminated (blue) cells. Outliers are depicted by black squares. Bud emergence occurs at time = 0. Data as in **Figure 6D.**

Figure 6 - Supplemental Figure 3: Transient Cdc24 recruitment can induce Cdc24-tdTomato accumulation, but cells can bud from an alternative position.

Representative fluorescence and phase time-course images for Cdc24-ePDZ transient recruitment when cells bud off target. Each image is 16.2 μm x 16.2 μm. Strain used: WYK8575.

Figure 7: Local Cdc24 recruitment induces precocious activation of Cdc42 that is dynamically maintained in the apparent absence of Bem1

A) Panels of representative cells depicting the response to dynamically re-positioned Cdc24 recruitment. Upper panels consist of phase contrast and fluorescent images and the lower panel is a kymograph. The laser was moved every 10 +/- 2 minutes throughout the cell cycle, as denoted by the white stars. Each image is 16.2 μm x 16.2 μm. Strain used: WYK8440.

B) Percentage of targeting events “Outcompeted” or “Not Outcompeted” relative to bud emergence (Time = 0). Time indicates when the target was moved to a new position relative to bud emergence. Data is binned by 5 minute time intervals, with the middle time point represented on the plot. The event was scored as “outcompeted” if Cdc42 activity dissipated from the original position and accumulated at the new position. Conversely, the event was

scored as "not outcompeted" if Cdc42 activity remained at the initial position upon target repositioning. Data are combined across multiple experiments (n total experiments > 2; n targeting events per time interval > 10; N total targeting events > 100; N total cells > 20).

C) Panels and a kymograph of a representative cell depicting the accumulation of Bem1 in response to dynamically re-positioned Cdc24 recruitment. Strain used: WYK8301.

D) Box-and-whisker plot denoting Bem1 accumulation in CDK1, *cdk1-as* + DMSO, and *cdk1-as* + 1NM-PP1 cells.

E) Time-course images of *cdk1-as* cells challenged with Cdc24 dynamic reorientation. Panels consist of phase contrast and either Cdc42-GTP or Bem1 accumulation psuedo-colored as a heat map. Cells were treated with either DMSO or 1NM-PP1 as denoted. Strains used: WYK8441 and WYK8442.

F) Quantification of dynamic reorientation in vehicle-treated or 1NM-PP1-treated *cdk1-as* cells. Described in **B**.

Figure 8: Localized recruitment of Cdc24 can overcome the polarity defect caused by actin depolymerization.

Accumulation kinetics for Cdc42-GTP or Bem1 in response to Cdc24 recruitment in the presence or absence of polymerized actin. All cells scored as "polarized" also undergo bud emergence within the course of the experiment (>100 minutes). Red lines represent cells exposed to light-induced Cdc24 recruitment. Blue lines represent mock-illuminated cells. Dark lines represent Vehicle-treated cells, while lighter-colored lines represent Latrunculin A-treated cells (see schematic).. Whi5 nuclear exit was used as a cell cycle marker and accumulation of Cdc42-GTP or Bem1 was scored relative to Whi5 exit. Data was binned by 5 minute intervals and combined across multiple experiments (n experiments = 2; N total cells > 40).

Figure 8 - Supplemental Figure 1: Loss of f-actin slows cell cycle entry.

Whi5 nuclear exit kinetics in Vehicle-treated (left) or LatrunculinA-treated (right) cells. Green lines refer to cells expressing the Cdc42 biosensor, while purple lines refer to cells expressing endogenous Bem1-tdTomato. Darker-colored lines represent mock-illuminated cells, while lighter-colored lines represent photo-activated cells (see schematic). Whi5 nuclear exit was slowed in LatA-treated cells. Data were binned by 5 minute intervals and combined across multiple experiments (n experiments = 2; N total cells > 40).

Figure 9: Nascent sites undergo competition to establish a single axis of polarity

A) Representative fluorescence and phase images in response to recruitment of Cdc24 to two sites simultaneously. Top panel depicts Cdc42-GTP response. Bottom panel depicts Bem1 response. Each image is 16.2 μm x 16.2 μm. Strains used: WYK8440 and WYK8301.

B) Percentage of cells with signal at one or both sites at any given time relative to bud emergence. Dark gray lines depict percentage of cells with activation at two sites simultaneously. Light gray lines represent percentage of cells with accumulation at only a single site. Bud emergence occurs at time = 0. Data are combined across multiple experiments (n experiments > 2; N total cells > 30 for each condition).

Figure 10: Working Model for polarity establishment.

In early G1, prior to Cdk1 activation, Cdc24, Bem1, and activated Cdc42 individually associate with the plasma membrane, but do not form stable complexes. With some frequency, Cdc24, and perhaps other Cdc42 GEFs, activate Cdc42 which can participate in a weak positive feedback loop with one or both GEFs. It is unclear whether Cdc42-GTP in early G1 interact with downstream effectors, such as Cla4, but if it does, it does not initiation Bem1 dependent positive feedback. Following Cdk1 activation, the Cla4-Bem1-Cdc24 complex assembles in late G1. This complex, may amplify the preexisting focus of Cdc42-GTP, and ultimately undergo strong

positive feedback to generate a single focus of Cdc42-GTP that subsequently triggers bud emergence.

Video 1

Photo-recruitment of Cdc24 is sufficient to activate Cdc42 and bias the bud site.

Representative phase contrast and fluorescent time-lapse images of the response to Cdc24 recruitment in cells expressing the Cdc42 biosensor. Left panel is the Nomarski image with the position of the target defined by the black circle. Right panel is the Cdc42 biosensor. fps = 10.

Video 2

Cdc42 activity can be dynamically repositioned in response to mobile sites of Cdc24 recruitment.

Representative phase contrast and fluorescent time-lapse images during dynamic repositioning experiments in cells expressing the Cdc42 biosensor. Left panel is the Nomarski image with the position of the target defined by the black circle. Right panel is the Cdc42 biosensor. fps = 10.

Video 3

Cdc42 activation can occur at two sites simultaneously in early G1.

Representative phase contrast and fluorescent time-lapse images in cells expressing the Cdc42 biosensor when challenged with two sites of Cdc24 recuritment. Left panel is the Nomarski image with the position of the target defined by the black circle. Right panel is the Cdc42 biosensor. fps = 10.

Video 4

Bem1 accumulation is limited to a single site of Cdc24 recruitment.

Representative phase contrast and fluorescent time-lapse images in cells expressing Bem1-tdTomato when challenged with two sites of Cdc24 recruitment. Left panel is the Nomarski image with the position of the target defined by the black circle. Right panel is the Cdc42 biosensor. fps = 10.